Composites Part B 202 (2020) 108416

Contents lists available at ScienceDirect

Composites Part B

journal homepage: www.elsevier.com/locate/compositesb

Nonlinear isogeometric multiscale simulation for design and fabrication of functionally graded knitted textiles

Huy Do [a,**], Ying Yi Tan [a], Nathalie Ramos [b], Josef Kiendl [c,b], Oliver Weeger [a,d,*]

[a] Singapore University of Technology and Design, SUTD Digital Manufacturing and Design (DManD) Centre, 8 Somapah Road, Singapore, 487372, Singapore
[b] Norwegian University of Science and Technology, Department of Marine Technology, Otto Nielsens veg 10, 7491, Trondheim, Norway
[c] Bundeswehr University Munich, Institute of Engineering Mechanics & Structural Analysis, Werner-Heisenberg-Weg 39, 85577, Neubiberg, Germany
[d] Technical University of Darmstadt, Cyber-Physical Simulation Group, Dolivostraße 15, 64293, Darmstadt, Germany

ARTICLE INFO

Keywords:
Machine knitting
Technical textiles
Nonlinear multiscale simulation
Isogeometric analysis
Functionally graded structures

ABSTRACT

We present a nonlinear multiscale modeling and simulation framework for the mechanical design of machine-knitted textiles with functionally graded microstructures. The framework operates on the mesoscale (stitch level), where yarns intermesh into stitch patterns, and the macroscale (fabric level), where these repetitive stitch patterns are composed into a fabric. On the mesoscale, representative unit cells consisting of single interlocked yarn loops, modeled as geometrically exact, nonlinear elastic 3D beams, are homogenized to compute their effective mechanical properties. From this data, a B-Spline response surface model is generated to represent the nonlinear orthotropic constitutive behavior on the macroscale, where the fabric is modeled by a nonlinear Kirchhoff–Love shell formulation and discretized using isogeometric finite elements. These functionally graded textiles with locally varying properties can be designed and analyzed by parameterizing the stitch value, i.e., the loop length of a single jersey stitch, and the knitting direction as mesoscopic design variables of the macroscopic response surface constitutive model. To validate the multiscale simulation and design approach, numerical results are compared against physical experiments of different tensile loading cases for various grading scenarios. Furthermore, the versatility of the method for the design of functionally graded textiles is demonstrated.

1. Introduction

Functional and technical textiles are an important class of materials not only in the fashion and apparel industries, but are also gaining traction in other domains ranging from aerospace and marine, architecture and civil engineering, and robotics and biomedical [1,2]. Among the other textile structure types, such as woven, non-woven, and braided, the act of fabricating a knitted textile probably offers the greatest potential for customizing and grading the textile's mechanical and functional properties [3]. Knitted fabrics possess a hierarchical structure that is typically categorized into three different scales: the micro-, meso- and macroscale. The microscale (*yarn level*) relates to the composition of a single *yarn*, which can consist of several different fibers or plies. A loop formed from a yarn by a single needle movement in the knitting process is called a *stitch*. The mesoscale (*stitch level*) relates either to a single stitch, e.g., single jersey, or a stitch pattern formed by multiple loops, e.g., double jersey. These stitch patterns are periodically repeated to form a fabric or textile, which constitutes the macroscale here (*textile level*). Variation of stitch patterns within a textile enables the creation of a complex topology with a three-dimensional (3D) geometry or advanced functionality [4]. Thus, the behavior of a knitted fabric can be tailored by changing its macroscopic shape, and also by varying and locally adapting its mesoscopic parameters such as stitch patterns, loop length, yarn material, and/or knitting orientation, see Fig. 1 for some examples.

Compared to other textile structures, relatively little computational engineering research has so far been dedicated to knitted textiles. This is mainly due to the high flexibility and low stiffness of knits made from traditional materials such as cotton, which makes them hardly relevant for structural engineering applications. However, this has changed in recent years due to the commercial availability of modern 3D knitting machines, which are also able to knit stiffer and functional materials, leading to the exploration of a larger variety of engineering applications. Moreover, there has been an increased interest in computer graphics and

* Corresponding author. Technical University of Darmstadt, Cyber-Physical Simulation Group, Dolivostraße 15, 64293 Darmstadt, Germany.
** Corresponding author.
E-mail addresses: huy_do@sutd.edu.sg (H. Do), weeger@cps.tu-darmstadt.de (O. Weeger).

https://doi.org/10.1016/j.compositesb.2020.108416
Received 11 May 2020; Received in revised form 1 September 2020; Accepted 14 September 2020
Available online 22 September 2020
1359-8368/

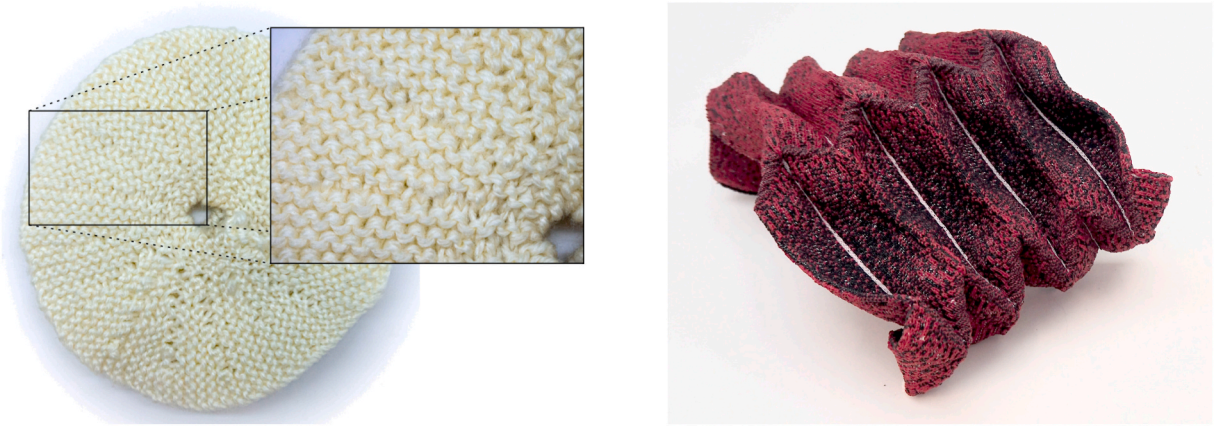

Fig. 1. Examples of knitted textiles with 3D shapes, graded stitch patterns and varying knitting directions.

computer-aided design communities where research has led to the development of new modeling tools to visualize and convert arbitrary 3D geometries into knitting machine instructions. Thus, this digital-to-physical translation broadens the design freedom of this fabrication technique, e.g. Refs. [5–10].

In the applied and computational mechanics communities, there has also been work done on the mechanical modeling of knitted textiles. However, this is particularly challenging due to the complex mechanical behavior of knits. This is due to geometric and contact interactions at the stitch level, which in turn results in highly nonlinear and orthotropic material behavior at the fabric level. At the mesoscale, geometrical models were introduced for stitch patterns such as the basic single jersey pattern [11,12]. These models were later used as the basis for the mechanical modeling of singular stitches, i.e., unit cells of the textile mesostructure, typically for the purpose of homogenization in the context of a multiscale simulation [13]. Furthermore, the use of analytical beam formulations [14–17], numerically discretized beam and beam-like models [18–20], as well as 3D solid finite element methods [21–26] have already been investigated to analyze the mechanical performance of the textile based on its mesoscale. On the macroscale, textiles and textile composites can be modeled as thin shells due to their relatively small thicknesses [27]. However, efficient sequential multiscale simulation requires homogenization [28] of the mesoscopic behavior into nonlinear, anisotropic constitutive models, which are difficult to develop. Thus far, several analytical [29,30] and response surface based [31,32] models have been presented in the context of (knitted) textiles and textile composites [25,33]. Some works also attempt the fullscale modeling of knitted textiles using finite element models based on the mesoscale, stitch level representation [34,35]. However, these methods require a high computational effort for the discretization of a significant number of loops and meshing of complex geometries and topologies.

Here, we propose a multiscale simulation approach that efficiently couples the macro- and mesoscales. The stitch level unit cells are modeled as geometrically exact, shear-deformable 3D beams [36] and are then homogenized into a response surface material model [32] that approximates the stress-strain relationship at the textile level as a B-Spline surface. In this way, we can efficiently generate a textile made out of the single jersey stitch pattern with localized regions of varying loop lengths [20]. Although we mostly focus on plane membranes here, the macroscale textile is modeled as a nonlinear Kirchhoff–Love shell, which is suitable for modeling thin shells without transverse shear deformation. It is discretized using an isogeometric finite element method [37], into which the nonlinear constitutive model is implemented [38]. Since the homogenization and macroscale simulation methods are not restricted to a specific mesoscale simulation method, one could potentially implement other models such as solid beam models with deformable cross-sections [39–41] or 3D solid finite elements into the framework.

Isogeometric analysis (IGA) methods [42,43] employ spline functions such as B-Splines and non-uniform rational B-Splines (NURBS). This has been done for geometric representation which is common in computer-aided design (CAD) systems, and also for the discretization of the numerical solution of a differential equation in the displacement field of the Kirchhoff–Love shell mid-surface. In this work, the IGA concept is extended to both the representation of the constitutive model as a B-Spline response surface and to the parameterization of additional design variables [44–47].

In this paper, we focus on graded knitted textiles made from a single jersey stitch pattern with two different knitting parameters: (1) loop length, which influences the stiffness; (2) the knitting direction, which determines the directions of anisotropy of the material model on the macroscale. To facilitate the computational design and analysis of functionally graded knitted textiles with locally varying properties, we include these mesoscopic properties as additional B-Spline surface parameter fields in the mechanical modeling approach. Except for the fullscale optimization approach presented in Ref. [16], we believe that a multiscale design concept which fully capitalizes on the potentials of customizing knitted textiles has yet to be proposed. In addition to introducing our computational design and simulation framework, we also validate our numerical methods against physical experiments with graded knitted textiles of increasing complexity, ranging from homogeneous knits at different loop lengths to fabrics that feature both graded loop lengths and varying knitting directions.

The structure of this manuscript is as follows: After this introductory Section 1, the numerical multiscale simulation framework and experimental methods are introduced in Section 2. Then, the results of the application and evaluation of the framework are presented and discussed in Section 3. We conclude with a summary and outlook in Section 4.

2. Methods

2.1. Isogeometric multiscale simulation framework

To model and simulate the mechanical behavior of knitted textiles, we adopt and extend the multiscale simulation approach introduced by some of the authors in Ref. [20].

2.1.1. Preliminaries on B-Splines and NURBS

The isogeometric parameterizations and discretizations used in this work are based on the formulation of curves and surfaces using B-Splines and NURBS. Here, we want to briefly introduce the most basic definitions, for a more elaborate discussion of the properties the interested

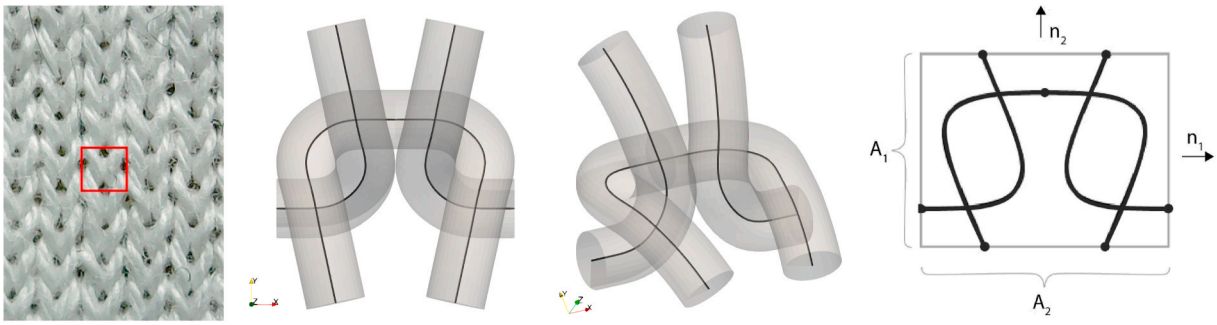

(a) Photo of a fabric (b) Solid in xy-plane view (c) Solid in a 3D view (d) Indication of $\mathbf{n}_1$ and $\mathbf{n}_2$

Fig. 2. Visualization of the unit cell of a single jersey stitch. Continuous lines indicate the centerline curves of the yarns, transparent solids the 3D beam cross-sections.

reader is refereed to Ref. [48].

In one dimension, B-Splines and NURBS basis functions are defined using a knot vector $\Xi = \{\xi_1,\ldots,\xi_m\}$, which is a non-decreasing sequence of knots $\xi_i \leq \xi_{i+1}$. For basis functions of degree $p > 0$, it is assumed that $\xi_1 = \ldots = \xi_{p+1} = 0$, $\xi_{m-p-1} = \ldots = \xi_m = 1$, i.e., that the knot vectors are *clamped* and thus the $n = m - p - 1$ basis functions are interpolatory at the end knots. The B-Spline basis functions $B_i : [0,1] \to \mathbb{R}$ can be recursively defined using the knot vector Ξ, the exact definition is omitted here, and introducing weights w_i they can be extended to NURBS basis functions:

$$N_i(\xi) = \frac{w_i B_i(\xi)}{\sum_{i=1}^{n} w_i B_i(\xi)}. \tag{1}$$

A spline curve in 3-dimensional space $\mathbf{c} : [0,1] \to \mathbb{R}^3$ can be defined using n NURBS basis functions N_i and control points $\mathbf{c}_i \in \mathbb{R}^3$:

$$\mathbf{c}(\xi) = \sum_{i=1}^{n} N_i(\xi)\mathbf{c}_i, \ \xi \in [0,1]. \tag{2}$$

In 2D, and analogously in higher dimensions, tensor-product B-splines can be defined using two knot vectors Ξ_1, Ξ_2 as $B_{ij}(\xi_1,\xi_2) = B_i(\xi_1)B_j(\xi_2)$ and then with weights $w_{ij} > 0$ also NURBS basis functions:

$$N_{ij}(\xi_1,\xi_2) = \frac{w_{ij}B_{ij}(\xi_1,\xi_2)}{\sum_{i=1}^{n_1}\sum_{j=1}^{n_2} w_{ij}B_{ij}(\xi_1,\xi_2)}. \tag{3}$$

A spline surface in 3-dimensional space $\mathbf{s} : [0,1]^2 \to \mathbb{R}^3$ can be defined with $n_1 n_2$ 2D NURBS basis functions N_{ij} and control points $\mathbf{s}_{ij} \in \mathbb{R}^3$:

$$\mathbf{s}(\xi_1,\xi_2) = \sum_{i=1}^{n_1}\sum_{j=1}^{n_2} N_{ij}(\xi_1,\xi_2)\mathbf{s}_{ij}, \ (\xi_1,\xi_2) \in [0,1]^2. \tag{4}$$

Following these definitions, B-Splines, NURBS, and spline curves and surfaces are interpolatory at the endpoints of the parameter intervals, C^p inside knot intervals and C^{p-r} at internal knots of multiplicity $r > 0$.

2.1.2. Mesoscale, stitch level simulation

At the mesoscale, i.e., the level of individual loops or stitches, the yarns are modeled as geometrically exact, shear-deformable 3D beams and their geometry represents the unit cell of a single stitch of the *single jersey* stitch pattern.

2.1.2.1. Geometric modeling. In Vassiliadis et al. [11], a widely adopted geometric model for the centerline curve of a single jersey stitch was presented. As a physical knit, the loop length ℓ can be controlled in the knitting machine via its stitch value setting, and serves as a design parameter for the grading of knits in this study, see Sect. 2.2. In its digital form, the geometric model of the loop is parameterized in terms of its width and height dimensions. Thus, the corresponding parameters have to be derived from actual knits to generate the geometrical models, see Ref. [20]. The vassiliadis model consists of a piecewise continuous centerline curve description of the yarn and, here, is interpolated by four B-Spline curves $\mathbf{r}_0$, compare (2)

$$\mathbf{r}_0(\xi) = \sum_{i=1}^{n} N_i(\xi)\mathbf{r}_{0,i}, \tag{5}$$

with $n = 12$ B-spline basis functions N_i of degree $p = 4$, which are defined on the reference unit interval $\xi \in [0,1]$, and control points $\mathbf{r}_{0,i} \in \mathbb{R}^3$, such that $\ell = ||\mathbf{r}_0||$.

2.1.2.2. Mechanical modeling. The deformed centerline curve $\mathbf{r} : [0,\ell] \to \mathbb{R}^3$ and the orientation of the circular yarn cross-section, which is given by a rotation matrix field $\mathbf{R} : [0,\ell] \to SO(3)$, are the main kinematic variables that describe the mechanical model in terms of the geometrically exact, shear-deformable, Simo–Reissner beam theory. From these variables, the strains and stresses, and the force and moment resultants $\mathbf{n}$ and $\mathbf{m}$, respectively, can be computed, which are used to express the balance equations of linear and angular momentum:

$$\begin{aligned} \mathbf{n}' + \overline{\mathbf{n}} &= 0, \\ \mathbf{m}' + \mathbf{n} \times \mathbf{r}' + \overline{\mathbf{m}} &= 0, \end{aligned} \tag{6}$$

where $\overline{\mathbf{n}}$ and $\overline{\mathbf{m}}$ are applied axial line loads and moments, which can here stem only from contact interaction forces, and $\cdot'$ denotes the arc-length derivative. The beam model of such a unit cell of a single jersey stitch is visualized in Fig. 2.

As already indicated by (5), the kinematic fields of the beam are discretized as B-Spline or NURBS curves and the strong forms of the balance equation (6) are collocated in order to obtain the control points of the deformed configuration $\mathbf{r}$.

This isogeometric collocation method was introduced in Ref. [49] and extended to beam-to-beam, i.e., here yarn-to-yarn, contacts using a penalty formulation with frictional contacts [36,50]. However, when modeling yarns as beams effects such as the initial deformation, anisotropy and thinning of the yarn cross-sections may play an important role. As described in detail in Refs. [20], these are included in the contact formulation by heuristically determining a suitable nonlinear law for the scaling of the contact penalty force, that only mildly penalizes initial penetrations, and the sliding friction coefficient, which is here taken as $\mu = 0.15$.

2.1.2.3. Homogenization of effective behavior. Periodic boundary conditions with prescribed effective deformation gradients $\mathbf{F}^*$ are applied to the stitch pattern unit cell. Then, the resulting forces on the yarns are homogenized to characterize the effective constitutive model, i.e., the highly nonlinear and orthotropic relationship between strains and stresses, see Ref. [20]. Since a shell model is used on the macroscale, see Sect. 2.1.3, two-dimensional macroscopic deformation gradients $\mathbf{F}^*$ for

biaxial (*ba*) and pure shear (*ps*) strain states are prescribed:

$$\mathbf{F}^{*}_{ba} = \begin{pmatrix} 1+\varepsilon_{11} & 0 \\ 0 & 1+\varepsilon_{22} \end{pmatrix}, \quad \mathbf{F}^{*}_{ps} = \begin{pmatrix} 1 & \sin\gamma \\ 0 & \cos\gamma \end{pmatrix} \tag{7}$$

where $\varepsilon_{11}, \varepsilon_{22}$ are the prescribed tensile strains and γ is a prescribed shear angle. Then, the resulting homogenized first Piola–Kirchhoff stresses $\mathbf{P}^{*}$ are computed from the accumulated forces at the boundary points, $\mathbf{n}_1, \mathbf{n}_2$, and the boundary surface areas of the unit cell, A_1, A_2, see Fig. 2d:

$$\mathbf{P}^{*} = \begin{pmatrix} \mathbf{n}_{1,1}/A_1 & \mathbf{n}_{2,1}/A_2 \\ \mathbf{n}_{1,2}/A_1 & \mathbf{n}_{2,2}/A_2 \end{pmatrix}, \tag{8}$$

where $\mathbf{n}_{i,j}$ refers to the j-th component of $\mathbf{n}_i$. The symmetric Green–Lagrange strain and 2nd Piola–Kirchhoff stress tensors can then be computed as:

$$\mathbf{E} = \frac{1}{2}(\mathbf{F}^{\top}\mathbf{F} - \mathbf{I}), \quad \mathbf{S} = \mathbf{F}^{-1}\mathbf{P}. \tag{9}$$

2.1.3. Macroscale, textile level simulation

On the macroscale, i.e., the level of a sheet of fabric, knitted textiles can be regarded as thin membranes or shells which exhibit large deformations due to their general flexibility. They also feature a complex, nonlinear, and orthotropic material response as a result of their microstructure. Thus, a membrane or shell model with nonlinear kinematics, finite strains, and a nonlinear constitutive law is to be used. This is realized with a nonlinear Kirchhoff–Love shell formulation which is discretized using an isogeometric finite element method, see Ref. [37].

2.1.3.1. Shell kinematics. Similarly to the beam model presented above, the kinematics of the shell are described only by its mid-surface $\mathbf{r}$, which is here parameterized as a 3-dimensional spline surface $\mathbf{r}(\theta_1, \theta_2) : \widehat{\Omega} \to \mathbb{R}^3$, $\widehat{\Omega} \subset \mathbb{R}^2$, compare (4). Using the two tangent vectors $\mathbf{a}_1, \mathbf{a}_2$ and the normal director $\mathbf{a}_3$ of the mid-surface

$$\mathbf{a}_\alpha = \mathbf{r}_{,\alpha} := \frac{\mathrm{d}\mathbf{r}}{\mathrm{d}\theta_\alpha} \ (\alpha = 1, 2), \quad \mathbf{a}_3 = \frac{\mathbf{a}_1 \times \mathbf{a}_2}{|\mathbf{a}_1 \times \mathbf{a}_2|}, \tag{10}$$

any point $\mathbf{x}$ in the 3-dimensional shell continuum can be described by a point on the mid-surface $\mathbf{r}$ and the normal direction $\mathbf{a}_3$:

$$\mathbf{x}(\theta_1, \theta_2, \theta_3) = \mathbf{r}(\theta_1, \theta_2) + \theta_3 \mathbf{a}_3(\theta_1, \theta_2), \tag{11}$$

where $(\theta_1, \theta_2) \in \widehat{\Omega}$ and $\theta_3 \in [-0.5t, 0.5t]$, with t being the shell thickness. From these tangent vectors and their derivatives, metric coefficients $a_{\alpha\beta}$ and curvature coefficients $b_{\alpha\beta}$ can be computed:

$$a_{\alpha\beta} = \mathbf{a}_\alpha \cdot \mathbf{a}_\beta, \quad b_{\alpha\beta} = \mathbf{a}_{\alpha,\beta} \cdot \mathbf{a}_3. \tag{12}$$

Ultimately, the in-plane components of the Green–Lagrange strain tensor $\mathbf{E}$ of the shell continuum can be expressed in terms of the curvilinear coordinates of the mid-surface (θ_1, θ_2) and the thickness coordinate θ_3, see Ref. [37,38] for details:

$$E_{\alpha\beta} = \varepsilon_{\alpha\beta} + \theta_3 \kappa_{\alpha\beta}, \tag{13}$$

where the membrane strains are defined as $\varepsilon_{\alpha\beta} = \frac{1}{2}\left(a_{\alpha\beta} - \mathring{a}_{\alpha\beta}\right)$ and the bending strains as $\kappa_{\alpha\beta} = \mathring{b}_{\alpha\beta} - b_{\alpha\beta}$, where quantities with the ring accent $\mathring{\cdot}$ refer to the initial, undeformed configuration of the shell mid-surface $\mathring{\mathbf{r}}$.

2.1.3.2. Variational formulation. The Green–Lagrange strain tensor $\mathbf{E}$ is related to the second Piola–Kirchhoff stress tensor $\mathbf{S}$ using a constitutive model $\mathbf{S} \equiv \mathbf{S}(\mathbf{E})$ and then the resultants for membrane forces $\mathbf{n}$ and bending moments $\mathbf{m}$ are computed via integration over the thickness of the shell

$$\mathbf{n}(\theta_1, \theta_2) = \int_{-t/2}^{t/2} \mathbf{S}(\mathbf{E}) \, d\theta_3, \quad \mathbf{m}(\theta_1, \theta_2) = \int_{-t/2}^{t/2} \mathbf{S}(\mathbf{E}) \, \theta_3 \, d\theta_3. \tag{14}$$

The variation of the internal virtual work or elastic strain energy of the shell body is then formulated as:

$$\delta W_{\text{int}} = \int_{\widehat{\Omega}} \mathbf{n} : \delta\varepsilon + \mathbf{m} : \delta\kappa \, d\theta_1 \, d\theta_2, \tag{15}$$

from which isogeometric finite element formulations can be derived [37], in which the deformed mid-surface $\mathbf{r}$ is discretized as a spline surface, see (4).

Due to the nonlinear material behavior, the thickness integrals in (14) cannot be computed analytically as it is the case for linear and only geometrically nonlinear shell formulations. Instead, we adopt a numerical integration scheme where the Green-Lagrange strains are computed at 3 integration points through the thickness according to (13) and the stresses are obtained from the response surface for each integration point, see below.

2.1.3.3. Response surface material model. Simulating the mechanical behavior of textiles that undergo large strains and stresses requires a nonlinear material model $\mathbf{S}(\mathbf{E})$. Furthermore, due to the nature of the knitting process, the material exhibits orthotropic behavior, i.e., substantially different stiffness in course and wale directions. Here, a B-Spline response surface material model is used to represent the nonlinear, orthotropic constitutive behavior, see Ref. [32]. In this approach, it is assumed that the shear components of the plane Green–Lagrange strain $\mathbf{E}$ and the second Piola–Kirchhoff stress $\mathbf{S}$ are decoupled from the tensile strain the tensile stress components when the material is loaded along its orthotropic and pure shear directions. With the 1-axis and 2-axis referring to the course- and the wale-wise directions, respectively, $\mathbf{E}$ and $\mathbf{S}$ in Voigt vector notation read

$$\mathbf{E} = \begin{pmatrix} E_1 \\ E_2 \\ 2E_{12} \end{pmatrix}, \ \mathbf{S} = \begin{pmatrix} S_1 \\ S_2 \\ S_{12} \end{pmatrix} \equiv \begin{pmatrix} S_1(E_1, E_2) \\ S_2(E_1, E_2) \\ S_{12}(E_{12}) \end{pmatrix} \tag{16}$$

The two tensile stress components S_1 and S_2 are represented in terms of E_1, E_2 as B-Spline response surfaces, see (4), and the shear stress component S_{12} in terms of E_{12} as a B-Spline response curve, see (2). The coefficients of these surfaces and curves are obtained from the homogenization of the mesoscale model, see Sect. 2.1.2, by prescribing a certain biaxial or shear strain, see (7), and computing the resulting stresses, see (8). In fact, to interpolate the experimental data, the stress response surfaces are only implicitly defined in terms of the tensile strain components and both are parameterized on the parametric domain $(\xi_1, \xi_2) \in [0, 1]^2$:

$$\begin{pmatrix} S_1 \\ S_2 \end{pmatrix}(\xi_1, \xi_2) = \sum_{i=1}^{n_1} \sum_{j=1}^{n_2} N_{ij}(\xi_1, \xi_2) \begin{pmatrix} S_1 \\ S_2 \end{pmatrix}_{ij}, \quad \begin{pmatrix} E_1 \\ E_2 \end{pmatrix}(\xi_1, \xi_2) = \sum_{i=1}^{n_1} \sum_{j=1}^{n_2} N_{ij}(\xi_1, \xi_2) \begin{pmatrix} E_1 \\ E_2 \end{pmatrix}_{ij}. \tag{17}$$

For given (E_1, E_2), the strain B-Spline surface is inverted to obtain the corresponding parameters (ξ_1, ξ_2), which are then used to evaluate the (S_1, S_2) surfaces. Furthermore, for the linearization of the shell model the constitutive material tensor is required, which can readily be computed from the response surface representation and reads in Voigt notation:

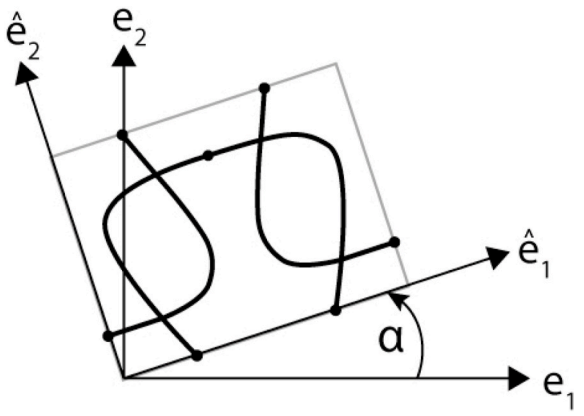

Fig. 3. Illustration of the angle α between the local Cartesian $\mathbf{e}_1$-direction and the knitting direction $\hat{\mathbf{e}}_1$, i.e., the course- or 1-direction of the material model.

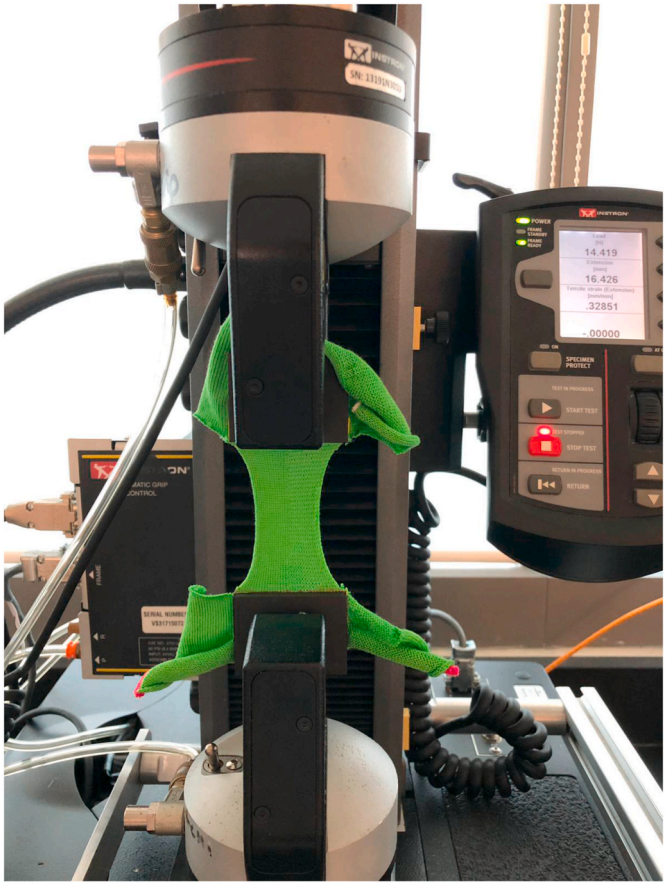

Fig. 4. Setup for tensile tests on 50×50 mm knitted fabric samples, here a wale-wise test of a patch with the discrete grading of loop length in course direction.

$$\mathbb{C}(\mathbf{E}) = \frac{\mathrm{d}\mathbf{S}}{\mathrm{d}\mathbf{E}} = \begin{pmatrix} \frac{\mathrm{d}S_1}{\mathrm{d}E_1} & \frac{\mathrm{d}S_1}{\mathrm{d}E_2} & 0 \\ \frac{\mathrm{d}S_2}{\mathrm{d}E_1} & \frac{\mathrm{d}S_2}{\mathrm{d}E_2} & 0 \\ 0 & 0 & \frac{\mathrm{d}S_{12}}{2\,\mathrm{d}E_{12}}. \end{pmatrix} \tag{18}$$

This 2-dimensional material model, which is homogenized from the planar behavior of a unit cell, can be directly used in (14) and the membrane forces $\mathbf{n}$ and bending moments $\mathbf{m}$ be computed using

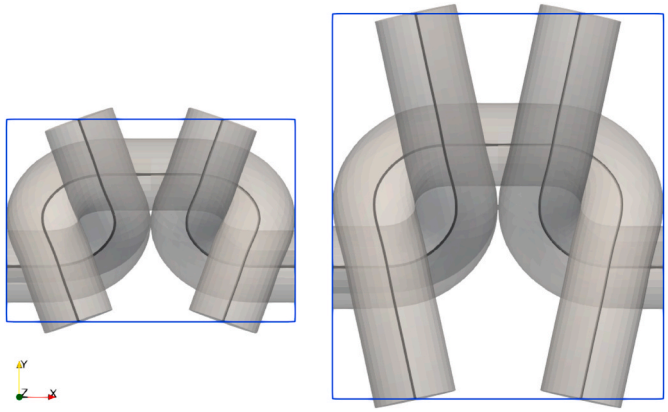

Fig. 5. Unit cells for $\ell = 4.5$ mm (left) and $\ell = 6.5$ mm (right). The bounding boxes with the nominal wale width w and course height c of the cells are shown in blue. (For interpretation of the references to color in this figure legend, the reader is referred to the Web version of this article.)

numerical integration. Hereby it is assumed that the textile is always stress-free in the lateral direction, i.e., an unknown $E_{33} \neq 0$ is maintained such that $S_{33} = 0$. This assumption is justified, since lateral contraction $F_{33} \neq 0$ is enabled by the choice of boundary conditions in (7), which results in $P_{33} = 0$ in (8). It should be highlighted that the response surface material model is *not* hyperelastic, since it is not based on the formulation of a strain energy density. Furthermore, it should be noted that the material model can generally be considered as nonlinear elastic, i.e., reversible. However, since friction is considered here in the mesoscale simulations, it should only be used for a one-time macroscale simulation with monotonic loading.

This shell model is then capable of not only simulating in-plane, membrane behavior, but also curved 3D geometries and bending deformation. However, the bending stiffness results from the through-the-thickness integration of the planar constitutive model, and thus probably over-estimates the actual bending stiffness of the textile. As such, we mainly focus our current investigations on planar textiles that are subjected to membrane stresses. Finally, we also show the evaluation of the bending behavior with the current model as an outlook, while the extension towards refined models that can incorporate the actual, homogenized bending stiffness of the textiles will be the subject of future work.

2.2. Multiscale design of graded knits

With the sequential multiscale simulation framework presented above, we are able to simulate large deformations and nonlinear orthotropic material behavior of knitted textiles. By fully exploiting the capabilities of knitting machines, it is possible to manufacture knits with locally varying knitting directions and stitch values and both these parameters influence the macroscopic constitutive model, see (16). For the design of such graded knits, the simulation framework is extended to analyze examples that feature variations of the above parameters.

2.2.1. Variation of knitting direction

Due to the knit mesostructure, the homogenized constitutive law on the fabric level is direction-dependent and expressed by equation (16) in the principal material directions. Normally, when (anisotropic) shell formulations are used, it is assumed that the material directions are identical to the local Cartesian coordinate system, here denoted as ($\mathbf{e}_1$, $\mathbf{e}_2$), to which the Green-Lagrange strain tensor from the curvilinear (θ^1, θ^2)-coordinate system, see (13), must be transformed, see Ref. [38] for further details.

However, here we want to enable the design of textiles with customized, varying knitting directions. Thus, the principal material

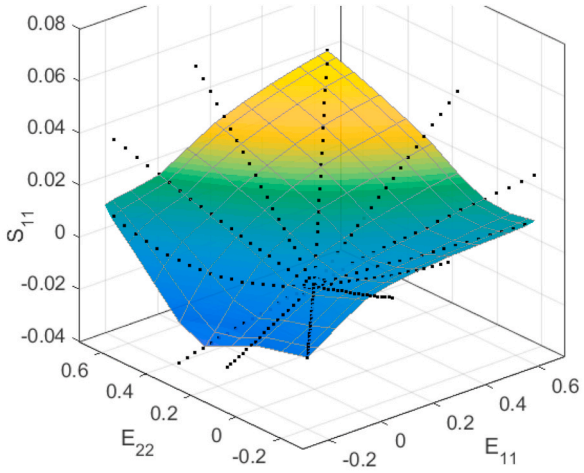

(a) $S_{11}(E_{11}, E_{22})$

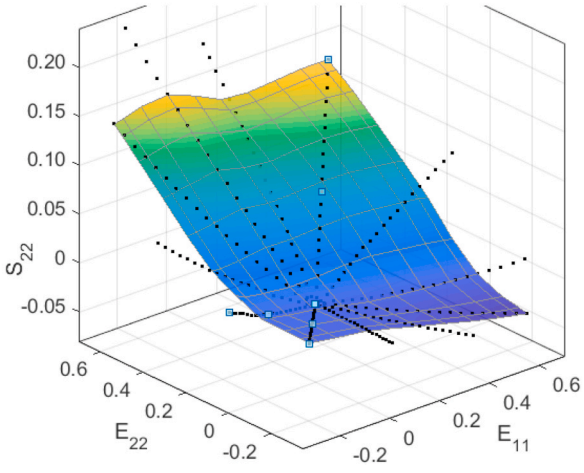

(b) $S_{22}(E_{11}, E_{22})$

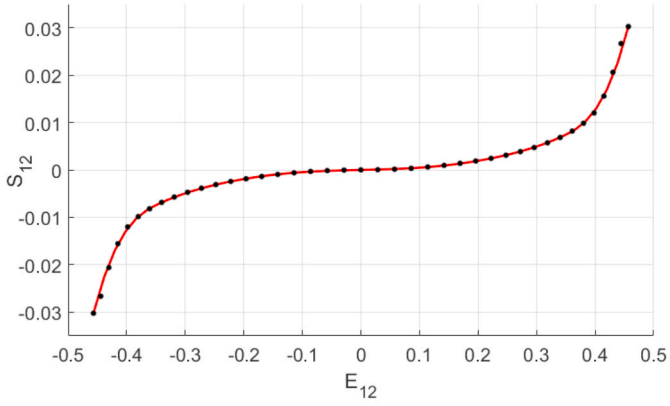

(c) $S_{12}(E_{12})$

Fig. 6. Stress response surfaces for single jersey with stitch value $\ell = 6.5$ mm (data points are shown as black dots).

directions $(\widehat{\mathbf{e}}_1, \widehat{\mathbf{e}}_2)$, the course and wale directions, do not have to be aligned with the local Cartesian basis. To address this design freedom, we parametrize the local orientation of the material model in terms of the angle between $\mathbf{e}_1$, which is aligned with $\mathbf{a}_1$, and the knitting direction $\widehat{\mathbf{e}}_1$, i.e., the course- or 1-direction of the material, as a spline surface $\alpha : \widehat{\Omega} \to \mathbb{R}$:

$$\alpha(\theta_1, \theta_2) = \sum_{i=1}^{n_1} \sum_{j=1}^{n_2} N_{ij}(\theta_1, \theta_2)\, \alpha_{ij}. \tag{19}$$

The definition of the angle α and orientation of the knitting direction are illustrated in Fig. 3.

Thus, the stresses, strains and constitutive material tensors have to be transformed between the local Cartesian coordinate system $(\mathbf{e}_1, \mathbf{e}_2)$ and the principal material coordinate system $(\widehat{\mathbf{e}}_1, \widehat{\mathbf{e}}_2)$. The details of these coordinate transformations are formulated in Appendix A in both tensor and Voigt notations and here only briefly stated. Using Voigt notation for $\mathbf{E}, \mathbf{S}, \mathbb{C}$, see (16), the transformations can be formulated in matrix form using a 3×3 transformation matrix $\mathbb{T}$, which reads for given angle α as:

$$\mathbb{T}(\alpha) = \begin{pmatrix} c^2 & s^2 & 2cs \\ s^2 & c^2 & -2cs \\ -cs & cs & c^2 - s^2 \end{pmatrix} \tag{20}$$

with the abbreviations $c := \cos\alpha$, $s := \sin\alpha$.

Following the approach proposed for the response surface material model by Ref. [32], the evaluation of the shell formulation with varying material orientation takes the following steps:

1. Evaluate $\mathbf{u}$ and the derivatives required for the evaluation of the Green–Lagrange strain tensor $\mathbf{E}$ at the material point (θ_1, θ_2), see (13)
2. Transform the Green–Lagrange strain tensor $\mathbf{E}$ and the curvatures onto the local Cartesian system $(\mathbf{e}_1, \mathbf{e}_2)$
3. Evaluate $\alpha(\theta_1, \theta_2)$ and determine the rotation matrix $\mathbb{T}(\alpha)$ from (20)
4. Rotate the strain tensor to the principal material directions:

$$\widehat{\mathbf{E}} = \mathbb{T}^{-\top} \mathbf{E} \tag{21}$$

5. Obtain the stress tensor $\widehat{\mathbf{S}}(\widehat{\mathbf{E}})$ and the constitutive tensor $\widehat{\mathbb{C}} = \frac{d\widehat{\mathbf{S}}}{d\widehat{\mathbf{E}}}$ in the principal material directions from the response surface constitutive model, see (16) and (18)
6. Transform the stress and constitutive tensors back to the local Cartesian system:

$$\mathbf{S} = \mathbb{T}^{-1}\, \widehat{\mathbf{S}}, \quad \mathbb{C} = \frac{\mathrm{d}\mathbf{S}}{\mathrm{d}\mathbf{E}} = \mathbb{T}^{-1}\, \widehat{\mathbb{C}}\, \mathbb{T}^{-\top} \tag{22}$$

2.2.2. *Grading of stitch value*

The mechanical properties of knitted fabrics can also be influenced by its stitch value ℓ. For example, the greater the stitch value, the longer the length of a loop/stitch which leads to a "looser" stitch. This larger stitch size translates to a reduced mechanical stiffness of the overall textile compared to a smaller, "denser" stitch. In modern knitting machines, the stitch value can be varied throughout a single knit, either discretely by assigning different patches of courses and wales with a certain stitch value, or continuously by slowly grading the stitch values.

To model designs with varying, graded stitch values, we introduce the scalar spline surface field $\ell : \widehat{\Omega} \to \mathbb{R}$:

$$\ell(\theta_1, \theta_2) = \sum_{i=1}^{n_1} \sum_{j=1}^{n_2} N_{ij}(\theta_1, \theta_2)\, \ell_{ij}, \tag{23}$$

as a design variable, that is parameterized in the curvilinear coordinate system of the shell.

To consider the variation of the stitch value ℓ in the mechanical properties, the response surface material model from (17) has to be parameterized in terms of the stitch value:

$$\mathbf{S}(\mathbf{E}, \ell) = \sum_{i=1}^{n_1} \sum_{j=1}^{n_2} N_{ij}(\mathbf{E})\, \mathbf{S}_{ij}(\ell). \tag{24}$$

The control points $\mathbf{S}_{ij}(\ell)$ of the response surface are now dependent on

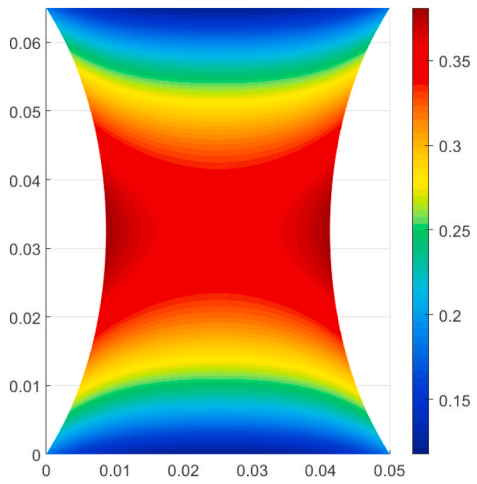

(a) Wale-wise tensile simulation for $\ell = 4.5$ mm at 20% strain (colored by E_{22})

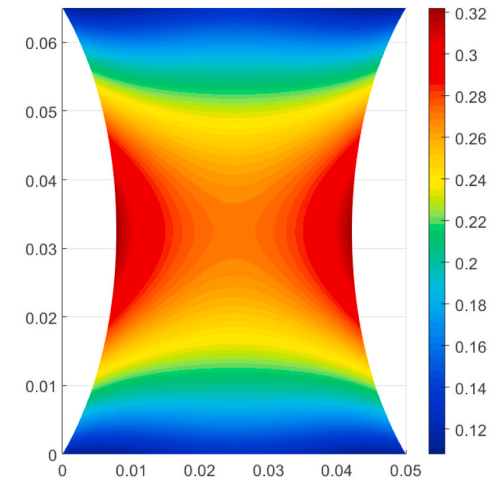

(b) Wale-wise tensile simulation for $\ell = 6.5$ mm at 20% strain (colored by E_{22})

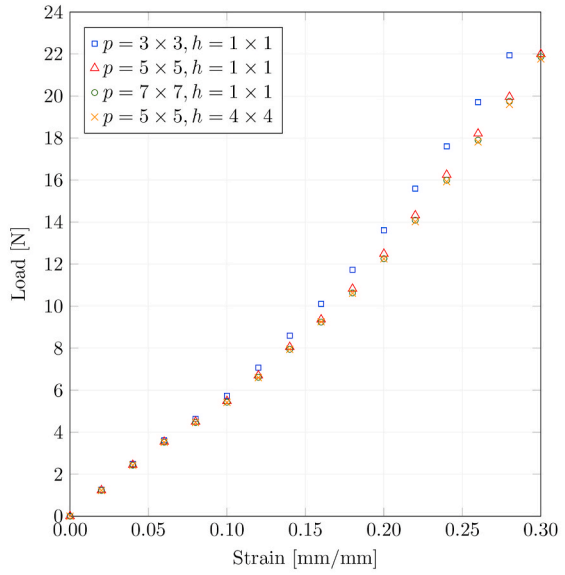

(c) Convergence study for wale-wise simulation of a patch with $\ell = 4.5$ mm

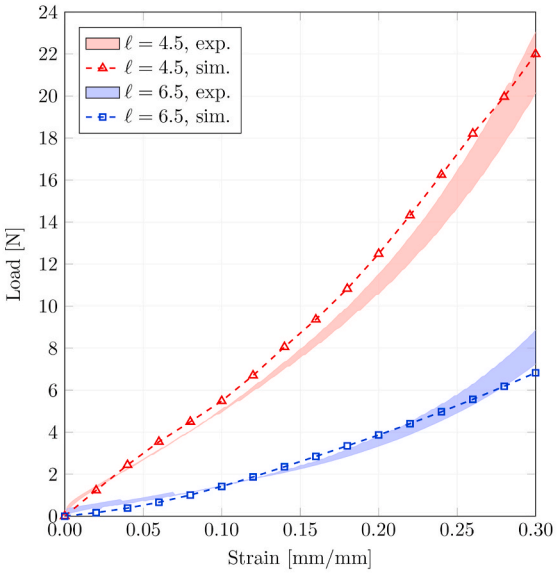

(d) Load-strain curves for wale-wise multiscale simulations and physical experiments

Fig. 7. Validation of simulation framework for uniform single jersey knits with stitch values of 4.5 and 6.5 mm.

the loop length ℓ. Thus, they can again be expressed as a spline curve:

$$\mathbf{S}_{ij}(\ell) = \sum_{k=1}^{n_3} N_k(\ell)\, \mathbf{S}_{ij,k}, \tag{25}$$

This interpolates a set of response surface control points obtained for given loop length values, e.g. $\ell = 4.5, 5.0, \ldots, 6.5$ mm, which is the result of the homogenization of mesoscopic unit cells with those loop lengths.

2.3. Fabrication and testing

For the validation and application of the above introduced multiscale simulation and design framework, we fabricate textile samples using a Shima Seiki MACH2XS153 WholeGarment knitting machine with a needle size of 15 gauge (i.e. 15 needles in an inch). All samples are knitted from a 2-ply Ne 20/2's ring-spun cotton yarn, with a linear density of 59.1 Tex, and in the single jersey stitch pattern. For the yarn, its diameter $d = 0.38$ mm and the Young's modulus $E = 800$ MPa are measured and used in the mesoscale simulations. Variations of the loop length per stitch are directly specified via the machine's i-DSCS automated yarn delivery control system.

Mechanical tests are carried out on an Instron 5943 universal testing machine with 1 kN load cell, see Fig. 4. For this purpose, the tested samples were cut from larger knitted fabrics to create a standardized square patch size of $L = 50$ mm can be clamped by the pneumatic jaws of the tensile testing machine. In all tests and relevant figures following in Sect. 3, a strain $\varepsilon = \Delta/L$ was applied to the samples via a cross-head displacement Δ and the resulting load f in N was measured. This force is converted into an effective tensile stress $\sigma = f/(L \cdot t)$, where $t = 2d$ is the thickness of the textile.

3. Results and discussion

The nonlinear multiscale simulation framework is applied to the design of functionally graded knits with varying stitch values and knitting directions and also validated against physical tests. For all examples and applications presented here, the geometric, material, fabrication, and testing specifications are followed as outlined above in Sect. 2.3. The simulations are performed on a desktop PC with an Intel © Core ™ i7-5930K CPU (3.5 GHz, 6 cores, 12 threads) and 32 GB RAM. The

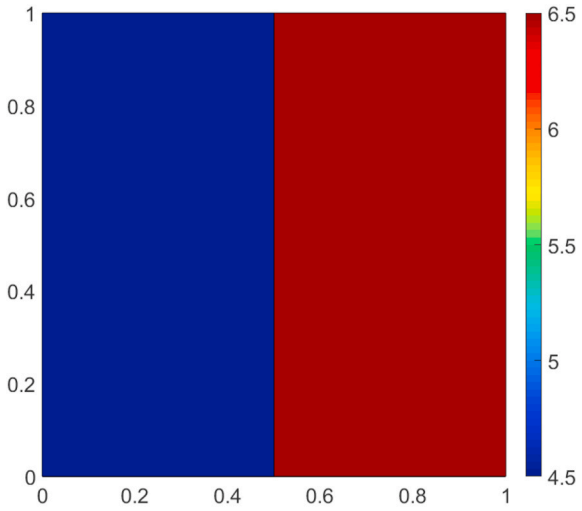

(a) Stitch value parameter field

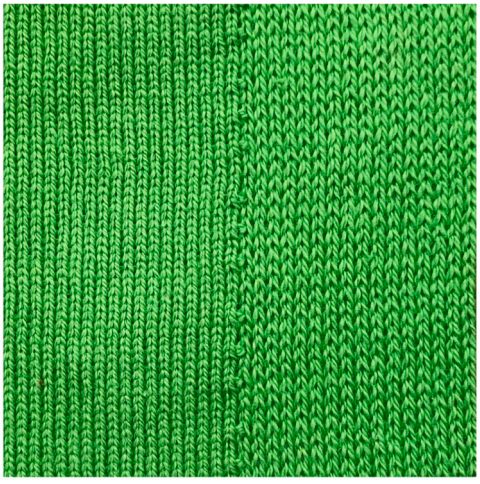

(b) Photo of a knitted fabric patch

Fig. 8. Course-wise graded fabric with discontinuous stitch value: 4.5 mm for left part, 6.5 mm for right part.

mesoscale homogenization is implemented in a C++ code. It takes around 30 min to generate the data for the response surface for one loop length (13 load cases with 20 incremental load steps each). The macroscale simulation is implemented in MATLAB © and one simulation with 15–20 load steps takes around 15 min.

3.1. Validation of the simulation framework

3.1.1. Homogenization of response surfaces

First, the multiscale simulation procedure, i.e., the homogenization of mesoscale simulations to obtain the response surface material models is applied to single jersey knits with loop lengths from $\ell = 4.5$ mm to $\ell = 6.5$ mm.

The unit cells for loop lengths of 4.5 and 6.5 mm, which result from the geometrical model outlined in Sect. 2.1.2, are shown in Fig. 5. With a wale width of $w = 1.26$ mm and course height $c = 0.88$ mm, the 4.5 mm loops are much smaller and thus denser than the 6.5 mm loops with $w = 1.41$ mm and $c = 1.64$ mm. Thus, the mechanical behavior and also the homogenized response surface material model at stitch value $\ell = 4.5$ mm is much stiffer than for $\ell = 6.5$ mm. Furthermore, due to the different aspect ratios of the microstructures, they have different degrees of anisotropy.

In Fig. 6, the obtained stress response surfaces for S_{11} and S_{22}, as well as the curve for S_{12} are visualized for stitch value 6.5 mm. The surfaces are approximating the data points generated from mesoscale simulations, which are shown as black dots in the plots. For all surfaces and curves, C^2-continuous B-Splines with degree $p = 3$ and $n = 11$ are used. The loop length dependent, parameterized response surfaces are then generated by interpolating the surfaces obtained for $\ell = 4.5, 5.0, \ldots, 6.5$, as outlined in Sect. 2.2.

3.1.2. Uniform, constant stitch values

The stress response surface models for constant loop lengths of 4.5 mm and 6.5 mm are first applied within the macroscale shell model and the multiscale simulations are validated against physical experiments.

Fabric patches of 50×50 mm size with uniform, constant stitch values of 4.5 mm and 6.5 mm are subjected to course- and wale-wise tensile tests, see Fig. 7, where (a) and (b) are showing the deformed shapes for only the wale-wise tensile test simulations at 30% strain. It can be observed that the different overall stiffnesses of the two fabrics and the anisotropy of their material behavior result in quite different strain distributions. For the applied strain of 30%, the maximum values of the Green–Lagrange strain E_{22} are ~37% and ~32% for 4.5 and 6.5 mm, respectively. In both cases, the maximum strains occur at the central boundaries of the patches, but for 4.5 mm the distribution along the central section appears to be more uniform than for 6.5 mm.

To ensure the accuracy of the macroscale simulation using the isogeometric shell formulation with the response surface material model, a convergence study is performed for the wale-wise tensile simulation of a patch with $\ell = 4.5$ mm, see Fig. 7c. B-spline discretizations with degrees $p = 3, 5, 7$ and $h = 1, 4$ elements in the knot vectors in both parametric directions are investigated. The overlap of the load-strain curves indicates that convergence of the numerical solution up to an "engineering accuracy" is obtained to a moderately high degree of $p = 5$ with only one element.

For the validation of the overall numerical framework, the load-vs.-strain curves of the simulation results for $p = 5 \times 5$, $h = 1 \times 1$ are compared against physical experiments with knitted samples, see Fig. 7d. To visualize the range of the load-strain curves obtained in experiments with 3–5 samples of the same type, the experimental results are shown as shaded areas that indicate the minimum and maximum loads observed in the tests. Overall, the numerical simulations are in good agreement with the physical wale-wise tensile tests for both stitch values and the deviations between simulations and experiments are within a similar range to the variations within the experimental results.

3.1.3. Discontinuously graded stitch value

In the first example for modeling graded textiles, we investigate a fabric patch with course-wise grading with distinct discontinuous stitch values: 4.5 mm for the left half and 6.5 mm for the right half. The stitch value distribution and a physical, knitted sample are shown in Fig. 8 (a) and (b), respectively. Computationally, the discontinuously graded fabric is modeled as a single NURBS patch. Alternatively, two patches with constant stitch value fields could be used, but this would require more elaborate techniques for multi-patch coupling, e.g., the bending strip method [51].

For the analysis and validation, the fabric is again subjected to tensile tests in both course- and wale-directions, i.e., horizontal and vertical directions, see Fig. 9. The course-wise tensile tests shown in Fig. 9a and (b) reveal that the strains E_{11} are much higher in the right half of the patch, which is to be expected since the loop length of 6.5 mm is generally less stiff than 4.5 mm. In the wale-wise simulation displayed in Fig. 9c and (d), the distribution of E_{22} is also more uniform in the right half. Both cases demonstrate a good qualitative agreement between the deformed shapes in simulations and experiments in terms of the patterns of lateral contractions (see Fig. 10).

(a) A physical course-wise tensile test at 30% strain

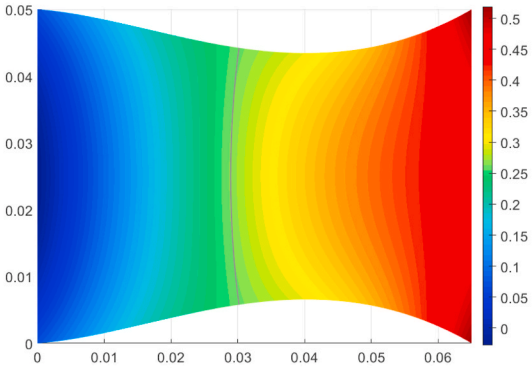

(b) Course-wise tensile simulation at 30% strain (colored by E_{11})

(c) A physical wale-wise tensile test at 30%

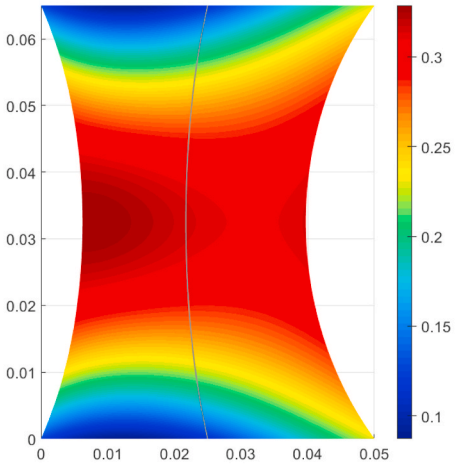

(d) Wale-wise tensile simulation at 30% strain (colored by E_{22})

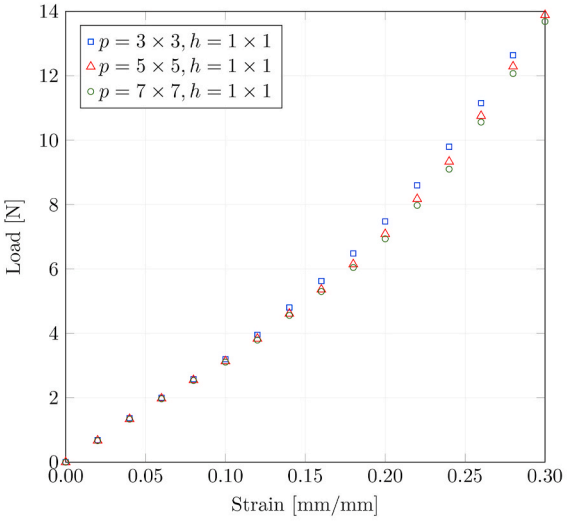

(e) Convergence study for wale-wise simulations

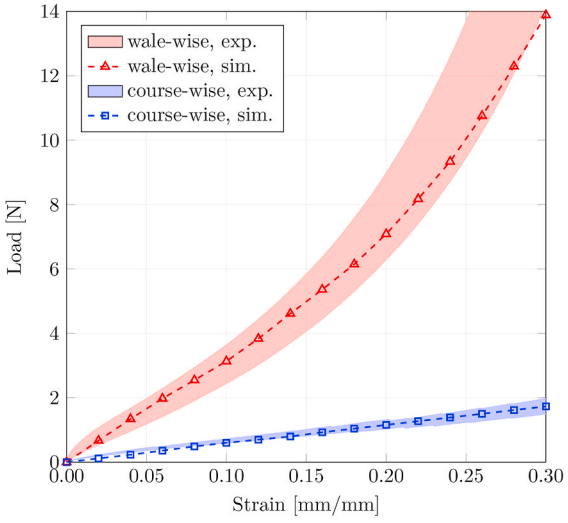

(f) Load-strain curves for course- and wale-wise multiscale simulations and physical experiments

Fig. 9. Course-wise graded fabric with discontinuous stitch value.

For these examples of discontinuously varying stitch value parameter field, the general accuracy of the macroscale simulations is once again investigated. In Fig. 9e, a convergence study is performed for the wale-wise test simulations, using degree $p = 3, 5, 7$ and $h = 1$ element. The load-strain curves are not much different and the solution with $p = 5$ is already sufficiently converged.

This discretization is then employed for a comparison of simulation results with physical tensile test experiments of the discontinuously graded fabric over a range of applied strains up to 30%, see Fig. 9f. Again, a good qualitative and quantitative agreement of the load-strain curves from multiscale simulations and experiments is achieved for both course- and wale-wise tests, as the simulated load-strain curves lie well

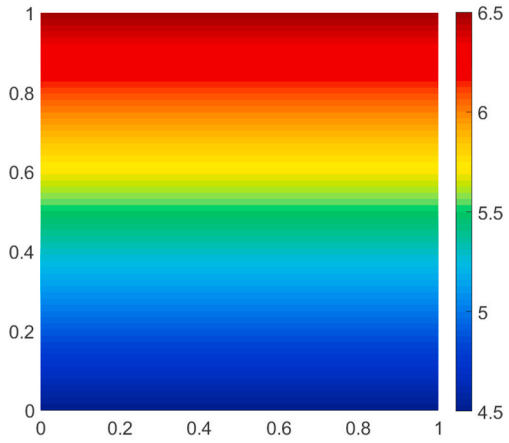

(a) Stitch value parameter field

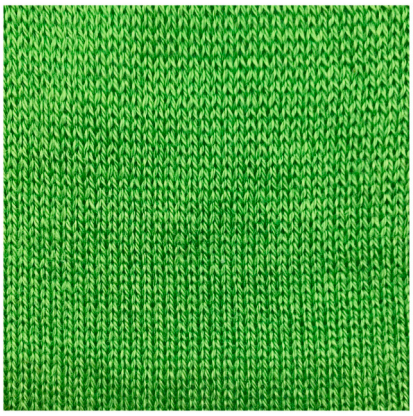

(b) Photo of knitted patch

Fig. 10. Wale-wise graded fabric with linearly varying stitch value: from 4.5 mm to 6.5 mm from bottom to top.

within the limits of the physical tests.

3.1.4. Linearly graded stitch value

Next, we introduce a knitted fabric with a linearly graded stitch value, which varies along the wale-direction from 4.5 mm at the bottom to 6.5 mm at the top of the patch. This is shown in Fig. 11, with stitch value field in (a) and the corresponding knitted sample in (b).

The deformed configurations of both course- and wale-wise tensile tests at 30% applied strain are shown for experiments with physical samples and the multiscale simulations in Fig. 11 (a)–(d). Again, there is a good qualitative agreement of the deformed shapes for both test cases, which can be seen from the lateral contractions of the initially square patches. Furthermore, as already noticed above, the areas with higher stitch values have lower stiffness and exhibit larger and more uniform strains.

Fig. 11e shows the comparison of the load-strain curves for tensile tests with physical samples of the discontinuous graded fabric and the multiscale simulation over a range of applied strains up to 30%. The simulated load-strain curves lie in between the lower and upper bounds of both experimental tensile tests along wale- and course-wise directions, and thus good agreement between the simulation and experimental results is achieved.

3.1.5. Knitting direction at 45°

With the final validation example, we demonstrate the parameterization of the orientation of the orthotropic material model in terms of the knitting direction. This involves the course direction corresponding with 1-direction of the material. A textile patch with a discontinuous grading of the stitch value, similar to Sect. 3.3, but instead with 4.5 mm in the bottom left half and 6.5 mm in the top right half is investigated, see Fig. 12. In addition to the stitch value grading, the patch has a knitting direction that is not aligned with the curvilinear θ^1-coordinate. As Fig. 12a indicates, the patch has a constant orientation of 45° between the course direction and the θ^1-direction, i.e., $\alpha \equiv \pi/4$. The parameterization of the stitch value and the knitting direction, indicated by the arrows pointing in the course direction, are visualized in Fig. 12a and a photo of a knitted patch is shown in (b).

The textile patch is subjected to a tensile test in the vertical direction, with the simulated deformed patches at 30% applied strain shown in Fig. 12 (c) and (d) and an example of a physical text in Fig. 12e. There is a reasonable agreement between the simulated shape of the deformed patch and the experimental example, which can be observed by the drawn diagonal line indicating the interface of the two regions. Also the comparison of the load-strain curves in Fig. 12f shows once again a good agreement of the multiscale simulations with physical tests on knitted samples, here for a combination of graded stitch parameter and rotated knitting direction.

3.1.6. Discussion of validations

In the preceding examples, uniaxial tensile tests were simulated, as such tests could also be realized experimentally for validation purposes. Since the textile patches are clamped at both ends in the direction of the applied deformation/strain, non-uniform lateral contractions (Poisson's effect) could be observed, which result in non-uniform strain and stress distributions with simultaneously occurring tensile and shear strains and stresses. Depending on the grading and orientation of the knitting direction, substantial differences and variations in strain patterns could be observed. Thus, these examples can be considered as well-suited to validate the nonlinear multiscale simulation framework and its application to functionally graded textile design.

For all investigated examples, good qualitative agreement of the shapes of the deformed textile patches in simulations and experiments could be observed. These are evident from the patterns of lateral contractions and other features of the deformations. However, a more quantitative comparison of the deformed shapes would be challenging since experimental results can be varying due to the inherent elasticity of the textiles and inaccuracies of the boundary conditions, as experimental samples had to be cut to size for the tests.

Instead, we have focused on the load-vs.-strain curves obtained from the experiments and simulations for quantitative comparisons. In general, very good agreements are observed as the simulated curves fall within the range of experimental results and also reproduced the trend of stiffening behavior for increasing strains. However, it could also be stated that the deviations increased for larger strains around 20–30%. Two potential causes might be the material model used for the mesoscale simulations with the beam model, see Sect. 2.1.2, is only linear and cannot represent any stiffening behavior of the yarn material, or the lack of coupling between tensile and shear strains and stresses within the macroscopic response surface material model, see Sect. 2.1.3. These aspects will be subject to future investigations.

3.2. Functionally graded design applications

After the validation of the multiscale simulation framework, we want to demonstrate the capabilities of the approach with further applications for the computational design of functionally graded knits with varying stitch values and knitting directions.

3.2.1. Bilinearly varying stitch value and direction

As a first design application, we introduce a planar, square fabric of size 50 × 50 mm, for which the stitch value and knitting direction are

(a) A physical course-wise tensile test at 30% strain

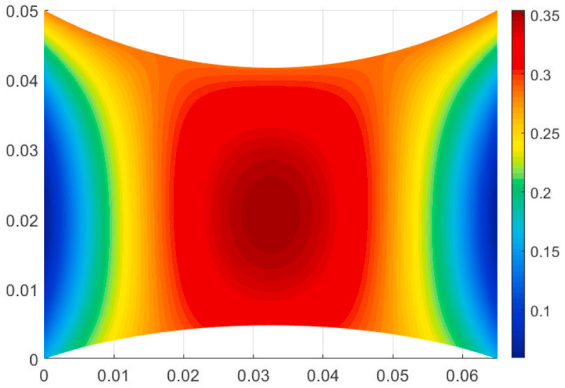

(b) Course-wise tensile simulation at 30% strain (colored by E_{11})

(c) A physical wale-wise tensile test at 30%

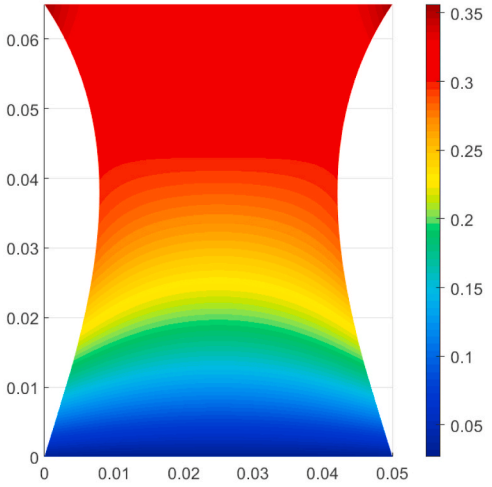

(d) Wale-wise tensile simulation at 30% strain (colored by E_{22})

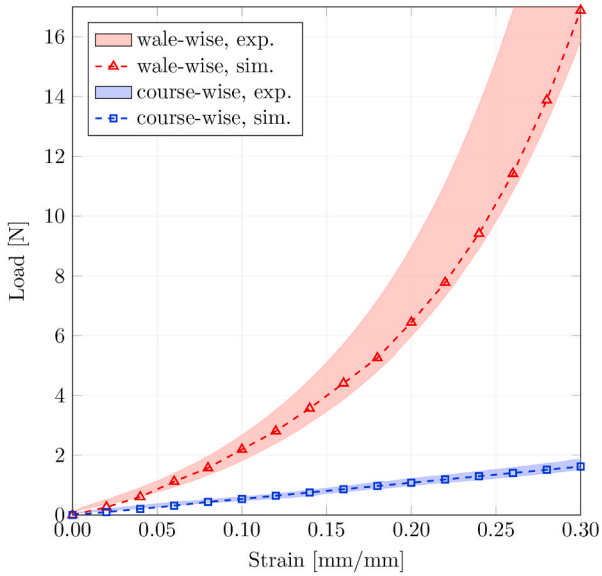

(e) Load-strain curves for course- and wale-wise multiscale simulations and physical experiments

Fig. 11. Wale-wise graded fabric with linearly varying stitch value: from 4.5 mm at the bottom to 6.5 mm at the top.

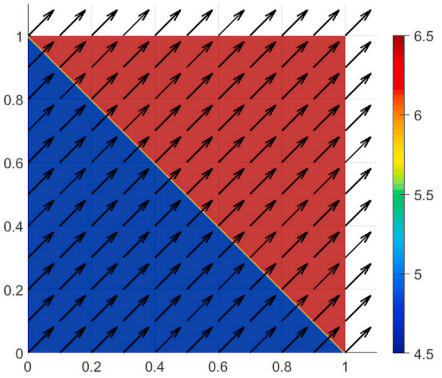

(a) Stitch value parameter field and knitting direction ($\alpha = \pi/4 = const.$)

(b) Photo of knitted patch

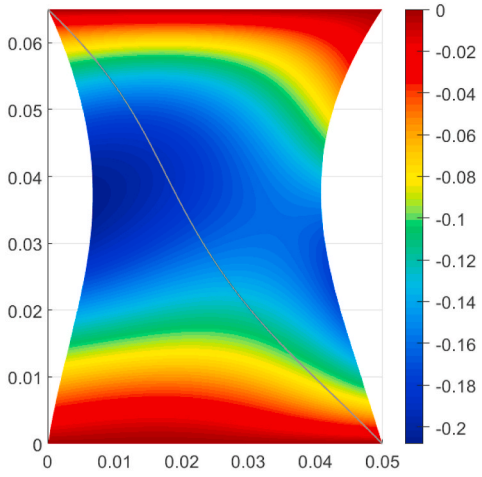

(c) Vertical tensile simulation at 30% strain (colored by E_{11})

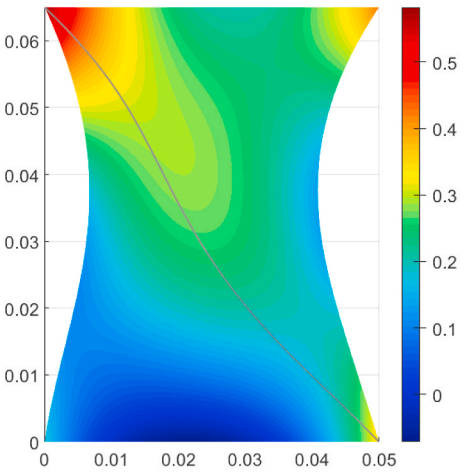

(d) Vertical tensile simulation at 30% strain (colored by E_{22})

(e) A physical tensile test at 30% strain

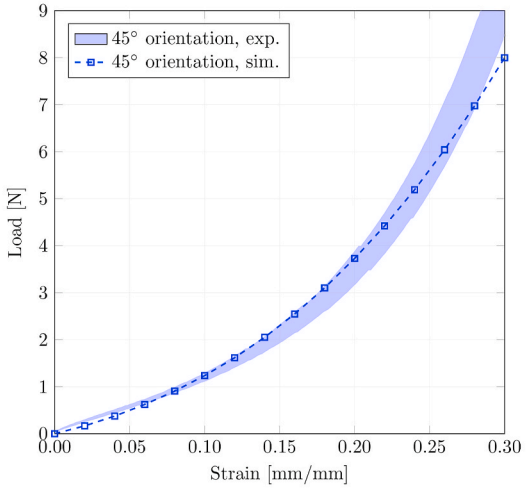

(f) Load-strain curves for multiscale simulation and physical experiments of vertical tensile test

Fig. 12. Course-wise graded fabric with discontinuous stitch value at 45°orientation.

both defined as bilinearly varying, i.e., with a B-Spline parameterization of degrees $p = 1 \times 1$, $h = 1 \times 1$ elements, and $n = 2 \times 2$ control points. The given values for both parameters at the four corners $(0,0), (1,0), (0,1), (1,1)$ of the patch are:

$$\ell = (4.5, 6.5, 6.5, 4.5) \text{ mm},$$
$$\alpha = (\pi/4, 0, \pi/2, \pi/4).$$

These parameter fields are visualized in Fig. 13, where the arrows in Fig. 13b indicate the course- or material-1-direction. The textile is symmetric with respect to the diagonal axis from bottom left to top right. Even with this simple, bilinear parameterization of the stitch value and knitting direction, a relatively complex textile microstructure could be realized.

Because of the symmetry of the material's microstructure, we

simulate the stretching of the textile along the diagonal direction. For this purpose, the degree of the B-Spline discretization is increased again to $p = 5 \times 5$. As boundary conditions, only the displacements of the bottom left corner are fixed as 0 and of the top right corner prescribed with $\mathbf{u}_1 = \mathbf{u}_2 = \varepsilon L > 0$.

Fig. 14 shows the results of the simulation in terms of the deformed shape of the fabric patch for a prescribed displacement of $\mathbf{u}_1 = \mathbf{u}_2 = 10$ mm, i.e., a diagonal strain of $\sqrt{2}\varepsilon = \sqrt{2}\cdot 0.2 \approx 28\%$, and the load-strain curve. As to be expected, the plots show that the strains E_{11} and E_{22} are anti-symmetric, while E_{12} is symmetric with respect to the diagonal. This serves as further validation of the multiscale simulation framework. Interestingly, in this example the load-strain curve is not stiffening for higher applied strains, see Fig. 14d, though the stretching happens along the diagonal, which is aligned with the knitting direction. This shows that by varying the material microstructure, i.e., loop length and knitting direction, textiles with non-standard deformation behavior can be realized.

3.2.2. Curved geometry with constant knit direction

In the next design application, we introduce a curved planar geometry and demonstrate the implications curved parameterizations have on the knitting direction, see Fig. 15. The geometry is described by a non-uniform NURBS parameterization with degrees $p = 3 \times 1$, $h = 1 \times 1$ elements and $n = 4 \times 2$ control points. The control points of the mid-surface and their weights are defined as:

$$\mathbf{r}^{\circ} = \begin{pmatrix} -\frac{1}{2} & -\frac{1}{6} & \frac{1}{6} & \frac{1}{2} & -\frac{1}{2} & -\frac{1}{6} & \frac{1}{6} & \frac{1}{2} \\ 0 & 0 & -\frac{1}{2} & -\frac{1}{2} & \frac{1}{2} & \frac{1}{2} & 0 & 0 \end{pmatrix} L, w = (1 \quad 2 \quad 2 \quad 1 \quad 1 \quad 2 \quad 2 \quad 1), \tag{26}$$

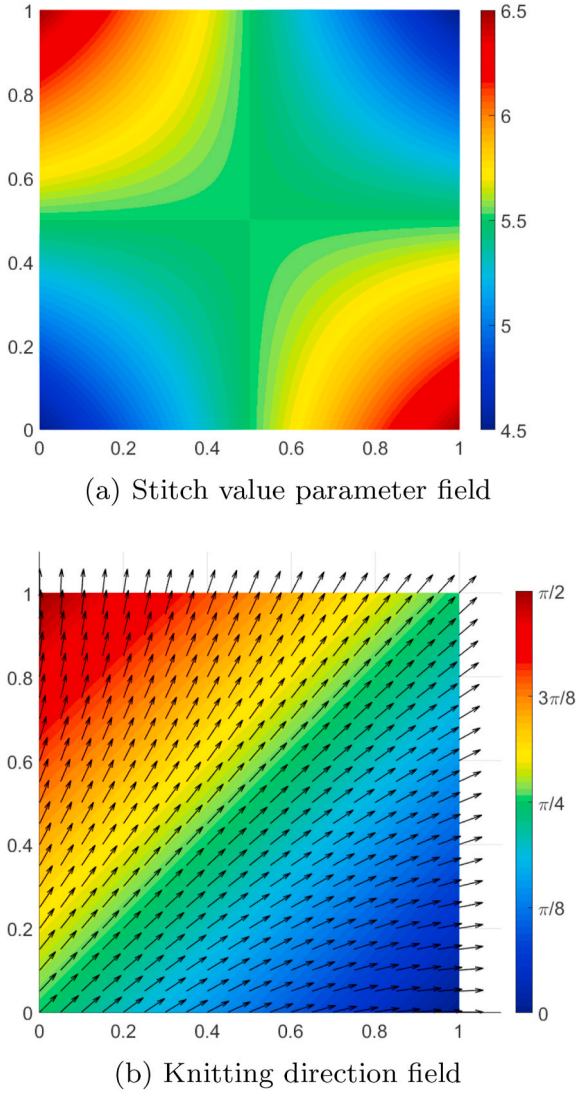

Fig. 13. Functionally graded textile with bilinearly varying stitch value and knitting direction.

with $L = 50$ mm. Furthermore, the stitch value field is parameterized with the same spline basis functions and a cubic grading in the θ_1-parameter direction is introduced with control point values $\ell = (4.5, 6.5, 6.5, 4.5)$ along that direction, see Fig. 15a.

For an angle of $\alpha \equiv 0$, the knitting direction follows the surface along the $\mathbf{e}_1$-direction of the local Cartesian coordinate system, which is aligned with the mid-surface tangent vector $\mathbf{r}^{\circ}_{,1} = \mathbf{a}^{\circ}_1$. However, here we want the knitting direction to be constant as the horizontal, physical x_1-direction, i.e., it should be aligned with the vector $(1, 0)^{\top}$, since this would make manufacturing simpler. Thus, we obtain the control points of the angle field $\alpha(\theta_1, \theta_2)$ such that the condition:

$$\begin{pmatrix} \cos\alpha & -\sin\alpha \\ \sin\alpha & \cos\alpha \end{pmatrix} \mathring{\mathbf{a}}_1(\theta_1, \theta_2) = \begin{pmatrix} 1 \\ 0 \end{pmatrix}, \tag{27}$$

is interpolated at the Greville abscissae. Since the angle field is parameterized with the same spline discretization with $p = 3 \times 1$, the knitting direction can not be exactly aligned with the x_1-direction everywhere in the domain, but very closely. Fig. 15b shows the values of α, which vary between 0 and $\pi/4$, the resulting knitting direction, which is indicated by the black arrows and almost constant, as well as the surface directors $\mathring{\mathbf{a}}_1$ as grey arrows.

For the simulation of a horizontal tensile test, the textile is fixed at the left boundary and uniform displacements are applied to the right boundary. In Fig. 15 the deformed configuration is visualized for an applied strain of 30% and the load-vs.-strain curve is plotted for the range from 0 to 40%. It can be seen that this large deformation of the curved, graded structure causes highly non-uniform strain patterns and a combination of high tensile and shear strains in the center of the fabric. The load-strain curve exhibits stiffening behavior with increasing strain, which is similar to the previous tensile tests.

3.2.3. Outlook on 3D textiles: bilinearly graded hyperbolic paraboloid

As discussed above at the end of Sect. 2.1.3, our simulation framework is also applicable to the design of 3-dimensional knitted textiles. However, simulating bending behavior within the shell and its material model would require further validation. Nevertheless, as the focus of this work is on the design parameterization aspects, we want to demonstrate an example of a 3D geometry with functionally graded parameters.

For this purpose, the planar patch of Sect. 3.2.1 is extended to 3D as a hyperbolic paraboloid with $x_3 = 0.24(x_1 - 2.5)(x_2 - 2.5)$ mm, i.e, the four corner points of the bilinear surface are moved up or down by 15 mm, as shown in Fig. 16a. For the bilinear grading of the microstructure,

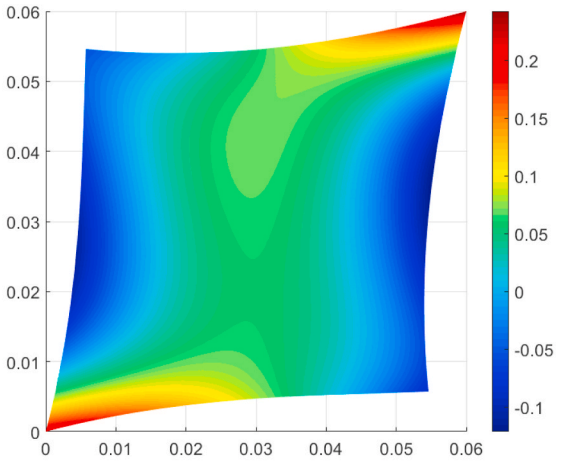

(a) Diagonal tensile simulation at $\sim 28\%$ strain (colored by E_{11})

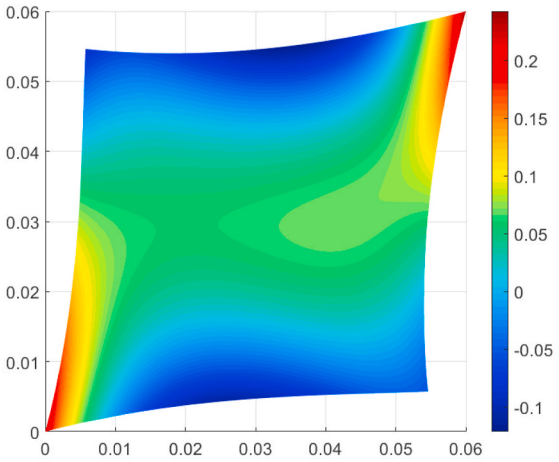

(b) Diagonal tensile simulation at $\sim 28\%$ strain (colored by E_{22})

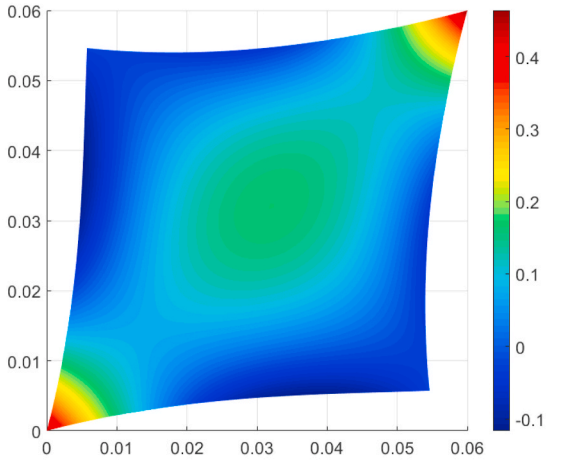

(c) Diagonal tensile simulation at $\sim 28\%$ strain (colored by E_{12})

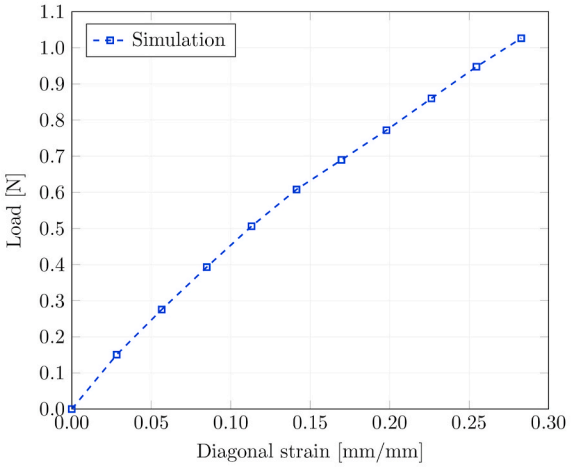

(d) Load-strain curve for multiscale simulation of diagonal tensile test

Fig. 14. Functionally graded 2D textile with varying stitch value and knitting direction.

the same definition of the stitch value and knitting direction as in Sect. 3.2.1, Fig. 13 is used. In Fig. 16b, the grading of the stitch value is indicated by the coloring, while the knitting direction is indicated by the arrows pointing in the course direction.

For the simulations, the boundary conditions are also chosen similarly to Sect. 3.2.1. The displacement of the bottom left corner is fixed in all three coordinates, for the top right corner it is prescribed to apply stretching or compression in x_1- and x_2-directions, but no deformation in x_3-direction, and for the bottom right and top left corners only the x_3-displacement is set to 0 to restrict rigid body motions of the surface.

Fig. 16c shows "tensile", diagonal stretching of the surface for an applied strain of $\sqrt{2}\cdot 0.15 \approx 21\%$ and Fig. 16d "compression" by $\sqrt{2}\cdot 0.1 \approx 14\%$. In both loading cases, the deformation of the surface is dominated by bending behavior, which can, of course, be seen from the deformed shapes, but also from the low values of the shear strains E_{12} and the tensile membrane strains E_{22} of the mid-surface that are provided in the figures. Thus, this demonstrates that the computational framework can generally also be applied to 3-dimensional textiles – with the reservation that the material model still has to be quantitatively verified for bending behavior.

4. Conclusions

In this work, a computational framework for nonlinear multiscale simulation and design of functionally graded, knitted textiles was presented and experimentally validated. The concept of isogeometric analysis was applied both for the NURBS discretization of the mesoscopic (stitch level) and macroscopic (fabric level) problems and also for the representation of the design parameters, namely the stitch values (loop lengths) of single jersey knits and the knitting direction, which defines the orientation of the highly orthotropic macroscale material model. Thus, this enables the computational multiscale design and functional grading of knitted textiles with spatially varying material properties.

The framework was realized by a combination of existing methods, namely the mesoscale modeling of single jersey stitches as geometrically exact beams and their discretization using an isogeometric collocation method; the homogenization of the mechanical behavior of these unit cells into an orthotropic response surface material model; and the macroscale modeling of the fabrics as nonlinear Kirchhoff–Love shells and their isogeometric finite element discretization.

For several examples with uniform parameters, graded stitch values, and varying orientations, the performance of this multiscale simulation framework was validated against experiments with physical knitted textile samples. Qualitative comparisons of the deformed shapes of the textiles in simulated and physical tensile tests, as well as quantitative comparisons of the load-vs.-strain curves showed good agreement and thus proved the accuracy of the method. Furthermore, its versatility for

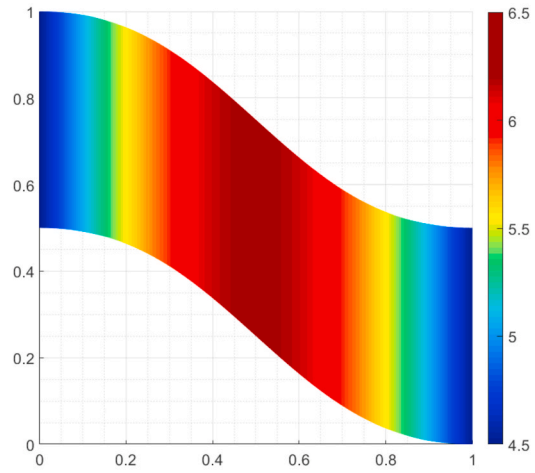

(a) Stitch value field

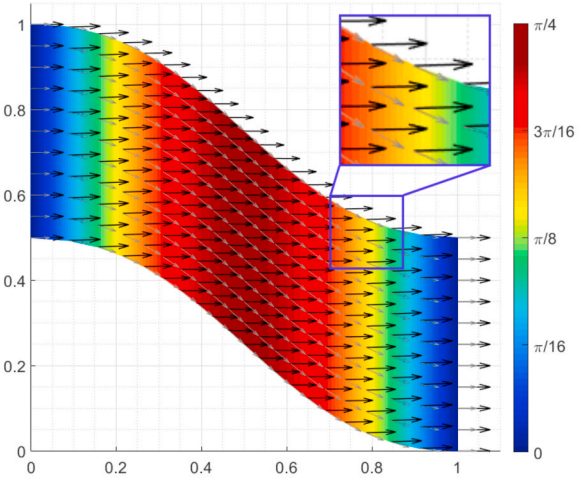

(b) Knitting direction field

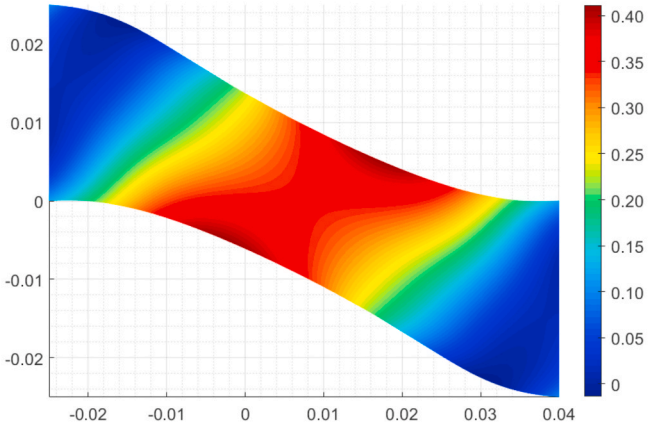

(c) Horizontal tensile simulation at 30% strain (colored by E_{11})

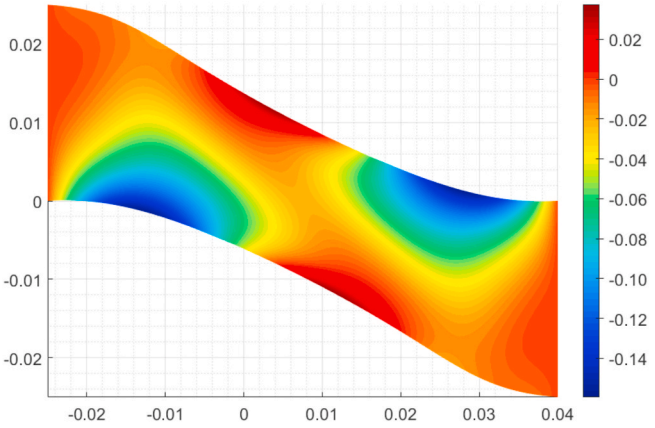

(d) Horizontal tensile simulation at 30% strain (colored by E_{22})

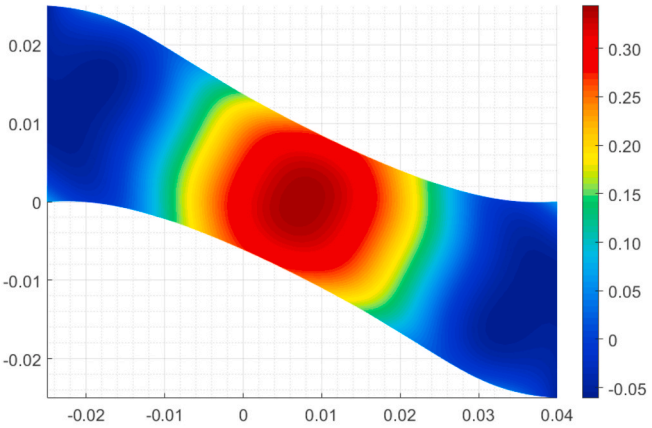

(e) Horizontal tensile simulation at 30% strain (colored by E_{12})

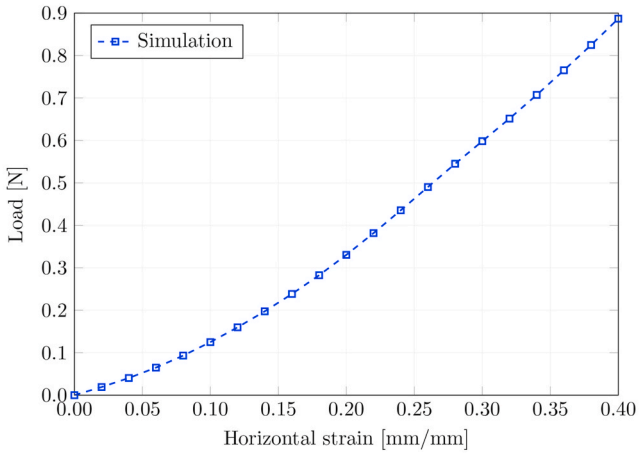

(f) Load-strain curve for multiscale simulation of horizontal tensile test

Fig. 15. Functionally graded, curved 2D textile with varying stitch value and physically constant knitting direction.

the design of functionally graded textiles with varying microstructure was demonstrated.

Some of the current limitations and potential future research directions were already mentioned and discussed above: The general accuracy of the multiscale simulations could be improved by including nonlinear, hyperelastic material behavior in the mesoscale model and by deriving and implementing a hyperelastic-orthotropic macroscale constitutive model that includes shear-tension coupling. For the simulation of 3-dimensional textiles, the accuracy of the current implementation of the macroscale constitutive model needs to be verified for bending behavior and, if necessary, modified such that the bending stiffness can also be homogenized from the mesoscale.

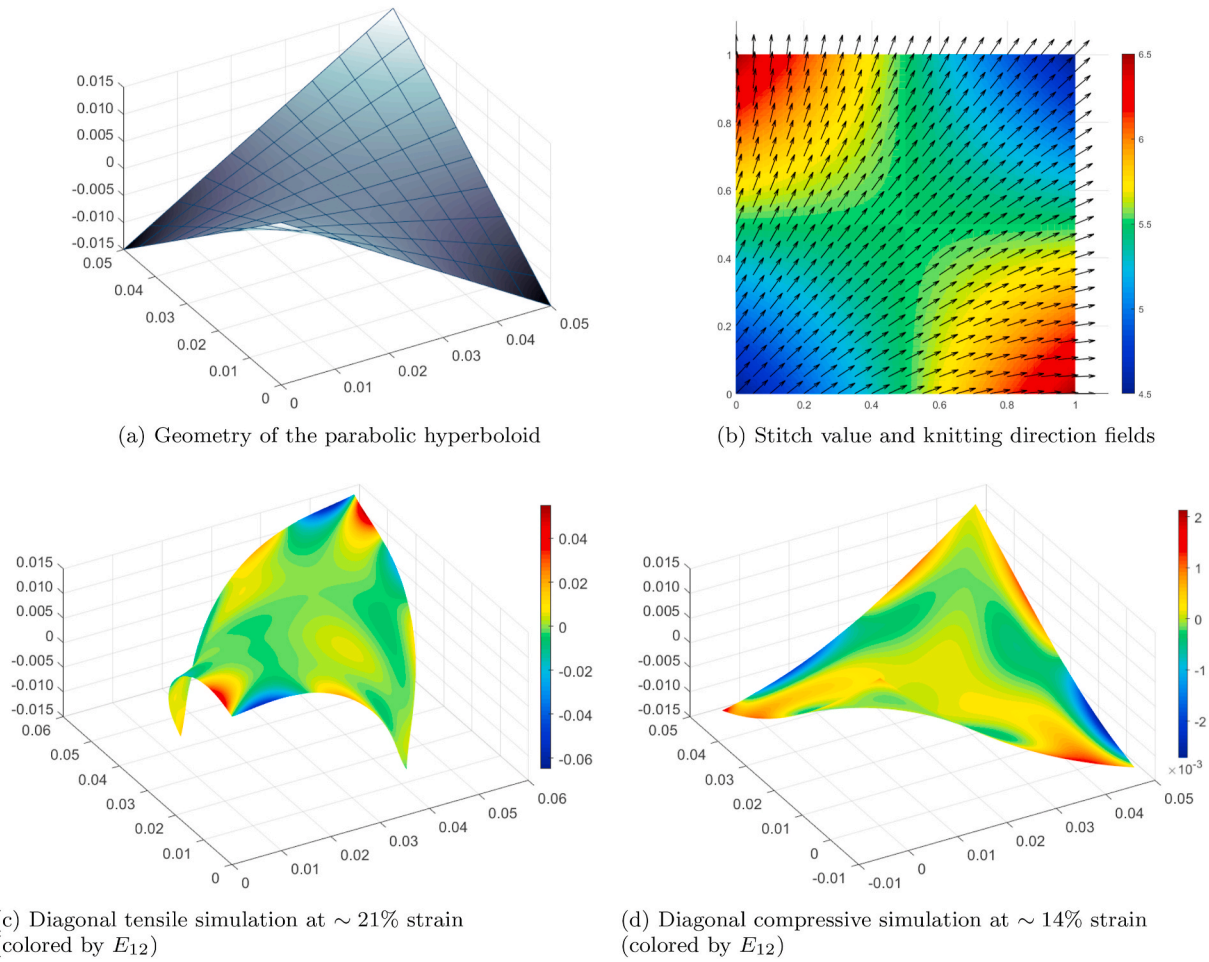

(a) Geometry of the parabolic hyperboloid

(b) Stitch value and knitting direction fields

(c) Diagonal tensile simulation at $\sim 21\%$ strain (colored by E_{12})

(d) Diagonal compressive simulation at $\sim 14\%$ strain (colored by E_{12})

Fig. 16. Functionally graded hyperbolic paraboloid with varying stitch value and knitting direction.

Furthermore, we would like to extend the microscale simulation and homogenization capabilities to other more geometrically complex stitch patterns, such as interlock or rib stitch patterns, and patterns formed using other loop types, including misses, tucks, etc. These could then be used for macroscopic simulations of textiles with varying stitch patterns. Furthermore, design optimization capabilities could be developed to optimize knitting parameters such that a desired mechanical behavior can be obtained by grading of a 3-dimensional textile.

Data availability

The authors provide access to the complete simulation data through the public GitHub repository https://github.com/CPShub/sim-data/.

CRediT authorship contribution statement

Huy Do: Conceptualization, Methodology, Software, Data curation, Validation, Visualization, Writing - original draft. **Ying Yi Tan:** Investigation, Data curation, Validation, Visualization, Writing - review & editing. **Nathalie Ramos:** Methodology, Software. **Josef Kiendl:** Methodology, Software, Writing - review & editing. **Oliver Weeger:** Conceptualization, Methodology, Software, Visualization, Writing - original draft, Supervision.

Declaration of competing interest

The authors declare that they have no known competing financial interests or personal relationships that could have appeared to influence the work reported in this paper.

Acknowledgements

The authors acknowledge support from the SUTD Digital Manufacturing and Design (DManD) Center, supported by the Singapore National Research Foundation.

Appendix A. Coordinate transformations

To evaluate the constitutive model in Sect. 2.1, the symmetric, second-order, 2×2 Green–Lagrange strain tensor E and 2nd Piola–Kirchhoff stress tensor S, as well as the symmetric, fourth-order, $2 \times 2 \times 2 \times 2$ constitutive tensor C have to be transformed between the local Cartesian coordinate system $(\mathbf{e}_1, \mathbf{e}_2)$ and the principal material coordinate system $(\widehat{\mathbf{e}}_1, \widehat{\mathbf{e}}_2)$. As indicated in Fig. 3, it holds:

$$\widehat{\mathbf{e}}_1 = \mathbf{Q}(\alpha)\, \mathbf{e}_1, \quad \widehat{\mathbf{e}}_2 = \mathbf{Q}(\alpha)\, \mathbf{e}_2, \tag{A.1}$$

where $\mathbf{Q}$ is the standard 2D rotation matrix:

$$\mathbf{Q}(\alpha) = \begin{pmatrix} \cos\alpha & -\sin\alpha \\ \sin\alpha & \cos\alpha \end{pmatrix}, \ \mathrm{Q}^{\top} \ \mathrm{Q} = \mathrm{I}. \tag{A.2}$$

Tensor notation. Then, the coordinate transformation of the symmetric strain and stress tensors can be expressed as:

$$\widehat{\mathbf{E}} = \mathbf{Q}^{\top}\mathbf{E}\mathbf{Q}, \quad \widehat{\mathbf{S}} = \mathbf{Q}^{\top}\mathbf{S}\mathbf{Q}, \tag{A.3}$$

where $\widehat{\cdot}$ indicates the transformed quantities in the material coordinate system. Since $\mathbf{Q}^{-1} = \mathbf{Q}^{\top}$, the inverse transformations read as:

$$\mathbf{E} = \mathbf{Q}\widehat{\mathbf{E}}\mathbf{Q}^{\top}, \quad \mathbf{S} = \mathbf{Q}\widehat{\mathbf{S}}\mathbf{Q}^{\top}. \tag{A.4}$$

Introducing a 4th order product"$\square$"of two 2nd order tensors $\mathbf{A}, \mathbf{B}$ as:

$$(\mathbf{A}\square\mathbf{B})_{ijkl} := A_{ik}B_{lj}, \tag{A.5}$$

which has the properties:

$$(\mathbf{A}\square\mathbf{B}) : \mathbf{C} = \mathbf{A}\mathbf{C}\mathbf{B}, \quad \frac{\partial(\mathbf{A}\mathbf{C}\mathbf{B})}{\partial\mathbf{C}} = \mathbf{A}\square\mathbf{B}, \tag{A.6}$$

when applied to a 2nd order tensor C, we can write:

$$\widehat{\mathbf{E}} = \mathbf{Q}^{\top}\mathbf{E}\mathbf{Q} = (\mathbf{Q}^{\top}\square\mathbf{Q}) : \mathbf{E} = \mathbb{T} : \mathbf{E}, \tag{A.7}$$

with the 4th order transformation tensor $\mathbb{T} := \mathbf{Q}^{\top}\square\mathbf{Q}$. Then, the constitutive tangent tensor can be calculated as:

$$\mathbb{C} = \frac{\mathrm{d}\mathbf{S}}{\mathrm{d}\mathbf{E}} = \frac{\partial\mathbf{S}}{\partial\widehat{\mathbf{S}}} : \frac{\partial\widehat{\mathbf{S}}}{\partial\widehat{\mathbf{E}}} : \frac{\partial\widehat{\mathbf{E}}}{\partial\mathbf{E}} = \frac{\partial\left(\mathbb{T}^{-1} : \widehat{\mathbf{S}}\right)}{\partial\widehat{\mathbf{S}}} : \widehat{\mathbb{C}} : \frac{\partial(\mathbb{T} : \mathbf{E})}{\partial\mathbf{E}} = \mathbb{T}^{-1} : \widehat{\mathbb{C}} : \mathbb{T}, \tag{A.8}$$

where $\mathbb{T}^{-1} = (\mathbf{Q}^{\top}\square\mathbf{Q})^{-1} = \mathbf{Q}\square\mathbf{Q}^{\top}$.

Voigt notation. Now, switching from proper tensor notation to the Voigt notation that applies to the symmetric strain and stress tensors and abusing the same symbols for the notation as $\mathbf{E}, \mathbf{S} \in \mathbb{R}^{3\times3}$ and $\mathbb{C} \in \mathbb{R}^{3\times3\times3\times3}$:

$$\mathbf{E} = \begin{pmatrix} E_{11} \\ E_{22} \\ 2E_{12} \end{pmatrix}, \quad \mathbf{S} = \begin{pmatrix} S_{11} \\ S_{22} \\ S_{12} \end{pmatrix}, \quad \mathbb{C} = \begin{pmatrix} C_{1111} & C_{1122} & C_{1112} \\ C_{2211} & C_{2222} & C_{2212} \\ C_{1211} & C_{1222} & C_{1212} \end{pmatrix} \tag{A.9}$$

as well as $\widehat{\mathbf{E}}, \widehat{\mathbf{S}} \in \mathbb{R}^3$ and $\widehat{\mathbb{C}} \in \mathbb{R}^{3\times3}$, one can express the coordinate transformations as:

$$\begin{aligned} \widehat{\mathbf{E}} = \mathbb{T}_E(\alpha)\,\mathbf{E} \quad \Leftrightarrow \quad \begin{pmatrix} \widehat{E}_{11} \\ \widehat{E}_{22} \\ 2\widehat{E}_{12} \end{pmatrix} &= \begin{pmatrix} c^2 & s^2 & cs \\ s^2 & c^2 & -cs \\ -2cs & 2cs & c^2 - s^2 \end{pmatrix} \begin{pmatrix} E_{11} \\ E_{22} \\ 2E_{12} \end{pmatrix}, \\ \widehat{\mathbf{S}} = \mathbb{T}_S(\alpha)\,\mathbf{S} \quad \Leftrightarrow \quad \begin{pmatrix} \widehat{S}_{11} \\ \widehat{S}_{22} \\ \widehat{S}_{12} \end{pmatrix} &= \begin{pmatrix} c^2 & s^2 & 2cs \\ s^2 & c^2 & -2cs \\ -cs & cs & c^2 - s^2 \end{pmatrix} \begin{pmatrix} S_{11} \\ S_{22} \\ S_{12} \end{pmatrix}, \end{aligned} \tag{A.10}$$

with the abbreviations $c := \cos\alpha$, $s := \sin\alpha$. Note that we have two different transformation matrices $\mathbb{T}_E$ and $\mathbb{T}_S$ here due to the factor 2 in the vector representation of E. However, $\mathbb{T}_S =: \mathbb{T}$ can be directly identified with the 4th order transformation tensor as defined above in (A.7). For the inverse transformations, the matrices are:

$$\begin{aligned} \mathbb{T}_E^{-1} &= \begin{pmatrix} c^2 & s^2 & -cs \\ s^2 & c^2 & cs \\ 2cs & -2cs & c^2 - s^2 \end{pmatrix} = \mathbb{T}_S^{\top}, \\ \mathbb{T}_S^{-1} &= \begin{pmatrix} c^2 & s^2 & -2cs \\ s^2 & c^2 & 2cs \\ cs & -cs & c^2 - s^2 \end{pmatrix} = \mathbb{T}_E^{\top}. \end{aligned} \tag{A.11}$$

Now, the 3×3-matrix representation of C can be calculated as:

$$\mathbb{C} = \frac{\mathrm{d}\mathbf{S}}{\mathrm{d}\mathbf{E}} = \frac{\partial\mathbf{S}}{\partial\widehat{\mathbf{S}}} \, \frac{\partial\widehat{\mathbf{S}}}{\partial\widehat{\mathbf{E}}} \, \frac{\partial\widehat{\mathbf{E}}}{\partial\mathbf{E}} = \frac{\partial\left(\mathbb{T}_S^{-1}\,\widehat{\mathbf{S}}\right)}{\partial\widehat{\mathbf{S}}} \, \widehat{\mathbb{C}} \, \frac{\partial(\mathbb{T}_E\,\mathbf{E})}{\partial\mathbf{E}} = \mathbb{T}_S^{-1} \, \widehat{\mathbb{C}} \, \mathbb{T}_S^{-\top} = \mathbb{T}^{-1} \, \widehat{\mathbb{C}} \, \mathbb{T}^{-\top}. \tag{A.12}$$

In summary, the necessary transformations required for evaluating $\mathbf{S}(\mathbf{E})$ and the tangent tensor $\mathbb{C}$ for given $\mathbf{E}$ are:

$$\widehat{\mathbf{E}} = \mathbb{T}^{-\top}\mathbf{E}, \quad \mathbf{S} = \mathbb{T}^{-1}\,\widehat{\mathbf{S}}, \quad \mathbb{C} = \mathbb{T}^{-1}\,\widehat{\mathbb{C}}\,\mathbb{T}^{-\top} \tag{A.13}$$

where only the "proper" matrix representation of the transformation $\mathbb{T} = \mathbb{T}_S$ is used, as in Sect. 2.2.1.

References

[1] Leong KH, Ramakrishna S, Huang ZM, Bibo GA. The potential of knitting for engineering composites—a review. Compos Appl Sci Manuf 2000;31(3):197–220.
[2] Chen X. Advances in 3D textiles. Number 167 in Woodhead Publishing Series in Textiles. Woodhead Publishing Limited; 2015.
[3] Spencer DJ, Knitting Technology. A comprehensive handbook and practical guide. Woodhead Publishing Limited; 2001.
[4] Abel J, Luntz J, Brei D. A two-dimensional analytical model and experimental validation of garter stitch knitted shape memory alloy actuator architecture. Smart Mater Struct August 2012;21(8):085011.
[5] Yuksel C, Kaldor JM, James DL, Marschner S. Stitch meshes for modeling knitted clothing with yarn-level detail. ACM Trans Graph 2012;31(4).
[6] McCann J, Albaugh L, Narayanan V, Grow A, Matusik W, Mankoff J, Hodgins J. A compiler for 3d machine knitting. ACM Trans Graph 2016;35(4).
[7] Leaf J, Wu R, Schweickart E, James DL, Marschner S. Interactive design of periodic yarn-level cloth patterns. ACM Trans Graph 2018;37(6).
[8] Wu K, Gao X, Ferguson Z, Panozzo D, Yuksel C. Stitch meshing. ACM Trans Graph 2018;37(4).
[9] Popescu M, Rippmann M, Van Mele T, Block P. Automated generation of knit patterns for non-developable surfaces. Singapore: Springer Singapore; 2018. p. 271–84.
[10] Narayanan V, Wu K, Yuksel C, McCann J. Visual knitting machine programming. 63:1–63:13 ACM Trans Graph 2019;38(4).
[11] Vassiliadis SG, Kallivretaki AE, Provatidis CG. Geometrical modelling of plain weft knitted fabrics. Indian J Fibre Text Res 2007;32:62–71.
[12] Kurbak A, Ekmen O. Basic studies for modeling complex weft knitted fabric structures part i: a geometrical model for widthwise curlings of plain knitted fabrics. Textil Res J 2008;78(3):198–208.
[13] Syerko E, Comas-Cardona S, Binetruy C. Models of mechanical properties/behavior of dry fibrous materials at various scales in bending and tension: a review. Compos Appl Sci Manuf August 2012;43(8):1365–88.
[14] Hong H, De Araujo MD, Fangueiro R, Ciobanu O. Theoretical analysis of load-extension properties of plain weft knits made from high performance yarns for composite reinforcement. Textil Res J 2002;72(11):991–6.
[15] Szablewski P, Korycki R. Deformation of cotton weft-knitted fabric subjected to tensile loads. J Nat Fibers December 2016;1(–11).
[16] Orlik J, Panasenko G, Shiryaev V. Optimization of textile-like materials via homogenization and beam approximations. Multiscale Model Simul 2016;14(2):637–67.
[17] Shiryaev V, Orlik J. A one-dimensional computational model for hyperelastic string structures with Coulomb friction. Math Methods Appl Sci 2017;40(3):741–56.
[18] Kyosev Y, Angelova Y, Kovar R. 3d modeling of plain weft knitted structures of compressible yarn. Research Journal of Textile and Apparel 2005;9(1):88–97.
[19] Duhovic M, Bhattacharyya D. Simulating the deformation mechanisms of knitted fabric composites. Compos Appl Sci Manuf November 2006;37(11):1897–915.
[20] Weeger O, Sakhaei AH, Tan YY, Quek YH, Lee TL, Yeung S-K, Kaijima S, Dunn ML. Nonlinear multi-scale modelling, simulation and validation of 3d knitted textiles. Appl Compos Mater 2018;25(4):797–810.
[21] de Araujo M, Fangueiro R, Hong H. Modelling and simulation of the mechanical behaviour of weft-knitted fabrics for technical applications. Autex Res J 2004;4(2).
[22] Vassiliadis SG, Kallivretaki AE, Provatidis CG. Mechanical simulation of the plain weft knitted fabrics. Int J Cloth Sci Technol March 2007;19(2):109–30.
[23] Fillep S, Mergheim J, Steinmann P. Computational modelling and homogenization of technical textiles. Eng Struct May 2013;50:68–73.
[24] Dinh TD, Weeger O, Kaijima S, Yeung S-K. Prediction of mechanical properties of knitted fabrics under tensile and shear loading: mesoscale analysis and its validation. Compos B Eng 2018;148:81–92.
[25] Sodhani D, Reese S, JockenhĀvel S, Mela P, Stapleton SE. Multi-scale modelling and simulation of a highly deformable embedded biomedical textile mesh composite. Compos B Eng 2018;143:6.
[26] Liu D, Koric S, Kontsos A. A multiscale homogenization approach for architectured knitted textiles. J Appl Mech June 2019:1.
[27] Hamila N, Boisse P, Sabourin F, Brunet M. A semi-discrete shell finite element for textile composite reinforcement forming simulation. Int J Numer Methods Eng September 2009;79(12):1443–66.
[28] Geers MGD, Kouznetsova VG, Brekelmans WAM. Computational homogenization. In: Multiscale modelling of plasticity and fracture by means of dislocation mechanics, CISM international Centre for mechanical sciences. Vienna: Springer; 2010. p. 327–94.
[29] Yeoman MS, Reddy D, Bowles HC, Bezuidenhout D, Zilla P, Franz T. A constitutive model for the warp-weft coupled non-linear behavior of knitted biomedical textiles. Biomaterials November 2010;31(32):8484–93.
[30] Lu T, Chen Z, Qi HJ, Wang TJ. A micro-structure based constitutive model for anisotropic stress–strain behaviors of artery tissues. Int J Solid Struct may 2018;139–140(55–64).
[31] Widhammer A. Variation of reference strategy – generation of optimized cutting patterns for textile fabrics. PhD thesis. Technische Universität München; 2015.
[32] Coelho M, Roehl D, Bletzinger K-U. Material model based on NURBS response surfaces. Appl Math Model November 2017;51:574–86.
[33] Thierry V, Brown L, Chronopoulos D. Multi-scale wave propagation modelling for two-dimensional periodic textile composites. Compos B Eng 2018;150:10.
[34] McKee PJ, Sokolow AC, Yu JH, Long LL, Wetzel ED. Finite element simulation of ballistic impact on single Jersey knit fabric. Compos Struct February 2017;162:98–107.
[35] Liu D, Christe D, Shakibajahromi B, Knittel C, Castaneda N, Breen D, Dion G, Kontsos A. On the role of material architecture in the mechanical behavior of knitted textiles. Int J Solid Struct 2017;109:101–11.
[36] Weeger O, Narayanan B, De Lorenzis L, Kiendl J, Dunn ML. An isogeometric collocation method for frictionless contact of Cosserat rods. Comput Methods Appl Mech Eng 2017;321:361–82.
[37] Kiendl J, Bletzinger K-U, Linhard J, Wüchner R. Isogeometric shell analysis with Kirchhoff-Love elements. Comput Methods Appl Mech Eng 2009;198(49–52):3902–14.
[38] Kiendl J, Hsu M-C, Wu Michael CH, Reali A. Isogeometric Kirchhoff–Love shell formulations for general hyperelastic materials. Comput Methods Appl Mech Eng 2015;291:280–303.
[39] Zivković M, Kojić M, Slavković R, Grujović N. A general beam finite element with deformable cross-section. Comput Methods Appl Mech Eng 2001;190(20):2651–80.
[40] Frischkorn J, Reese S. A solid-beam finite element and non-linear constitutive modelling. Comput Methods Appl Mech Eng October 2013;265(Supplement C):195–212.
[41] Gao S, Liang B, Vidal-Salle E. Development of a new 3d beam element with section changes: the first step for large scale textile modelling. Finite Elem Anal Des October 2015;104:80–8.
[42] Hughes TJR, Cottrell JA, Bazilevs Y. Isogeometric analysis: CAD, finite elements, NURBS, exact geometry and mesh refinement. Comput Methods Appl Mech Eng 2005;194(39–41).
[43] Cottrell JA, Hughes TJR, Bazilevs Y. Isogeometric analysis: towards integration of CAD and FEM. John Wiley & Sons; 2009.
[44] Hsu M-C, Wang C, Herrema AJ, Schillinger D, Ghoshal A, Bazilevs Y. An interactive geometry modeling and parametric design platform for isogeometric analysis. Comput Math Appl October 2015;70(7):1481–500.
[45] Benzaken J, Herrema AJ, Hsu M-C, Evans JA. A rapid and efficient isogeometric design space exploration framework with application to structural mechanics. Comput Methods Appl Mech Eng April 2017;316:1215–56.
[46] Herrema AJ, Wiese NM, Darling CN, Ganapathysubramanian B, Krishnamurthy A, Hsu M-C. A framework for parametric design optimization using isogeometric analysis. Comput Methods Appl Mech Eng April 2017;316:944–65.
[47] Weeger O, Yeung S-K, Dunn ML. Fully isogeometric modeling and analysis of nonlinear 3d beams with spatially varying geometric and material parameters. Comput Methods Appl Mech Eng 2018;342:95–115.
[48] Piegl LA, Tiller W. *The NURBS book*. Monographs in visual communication. Springer; 1997.
[49] Weeger O, Yeung S-K, Dunn ML. Isogeometric collocation methods for Cosserat rods and rod structures. Comput Methods Appl Mech Eng 2017;316:100–22.
[50] Weeger O, Narayanan B, Dunn ML. Isogeometric collocation for nonlinear dynamic analysis of Cosserat rods with frictional contact. Nonlinear Dynam 2018;91(2):1213–27.
[51] Kiendl J, Bazilevs Y, Hsu M-C, Wüchner R, Bletzinger K-U. The bending strip method for isogeometric analysis of Kirchhoff-Love shell structures comprised of multiple patches. Comput Methods Appl Mech Eng 2010;199(37–40):2403–16.